PERSPECTIVE

Check for updates

Hydrogen society: from present to future†

Daqin Guan, [ID] ‡[a] Bowen Wang,‡[abc] Jiguang Zhang, [ID] ‡[de] Rui Shi,[de] Kui Jiao, [ID] *[bc] Lincai Li,[b] Yang Wang,[b] Biao Xie,[b] Qingwen Zhang,[f] Jie Yu,[ag] Yunfeng Zhu, [ID] [de] Zongping Shao*[h] and Meng Ni [ID] *[a]

Hydrogen energy is an important cornerstone for realizing net-zero and sustainable development plans. The successful construction of a hydrogen society requires advancements in technology and the rational design of hydrogen production, storage, delivery, and usage. Herein, we provide systematic insights into the recent attainments, limitations, and future directions of the abovementioned aspects. With the development of renewable energy sources, sustainable green hydrogen production should replace the modes of traditional grey hydrogen and transitional blue hydrogen. Our techno-economic calculations reveal that high electricity consumption accounts for most of the costs of green hydrogen production, where different regional electricity prices induce hydrogen flows to bridge gaps in supply and demand. Fundamental rules and methodologies for catalyst morphologies, physiochemical properties, structural features, and screening pathways are provided to rationally exploit optimal electrocatalysts with low electricity consumption levels. Moreover, existing physical-based hydrogen storage systems with high acceptance and limited energy density can be replaced by promising material-based hydrogen storage systems for certain applications; these applications still face kinetic, thermodynamic, and engineering challenges. Ideal hydrogen delivery routes *via* trailers, pipelines, hydrogen carriers, and stationary hydrogen production systems strongly rely on specific scenarios. Our original calculation scenarios provide a good example for meeting the DOE cost target. We believe that this perspective will offer critical guidance for the future establishment of a hydrogen society.

Broader context

Hydrogen energy will exert critical and indispensable roles in production, living, the environment, and economy. The successful construction of a hydrogen society requires technological advancements and rational design of hydrogen production, storage, delivery, and usage. This paper carefully analyses and notes recent attainments, limitations, and future directions of hydrogen production, storage, delivery, and usage combined with some original techno-economic calculations. We hope that this perspective will provide critical guidance for future establishment of a hydrogen society and excite the immediate interest of a wide audience of economists, sociologists, materials scientists, chemists, physicists, engineers, and others who are interested in the future of hydrogen energy.

1. Background

The increasing demand for energy resources and the excessive consumption of nonrenewable fossil fuels have triggered many issues in energy and the environment (*i.e.*, energy shortage, global warming, ocean acidification and air pollution issues) since the industrial revolutions.[1] The development of green energy carriers and the exploration of sustainable energy

[a] *Department of Building and Real Estate, Research Institute for Sustainable Urban Development (RISUD) and Research Institute for Smart Energy (RISE), The Hong Kong Polytechnic University, Hung Hom, Kowloon 999077, Hong Kong, China. E-mail: meng.ni@polyu.edu.hk*

[b] *State Key Laboratory of Engines, Tianjin University, 135 Yaguan Rd, Tianjin 300350, China. E-mail: kjiao@tju.edu.cn*

[c] *National Industry-Education Platform of Energy Storage, Tianjin University, Tianjin 300350, China*

[d] *College of Materials Science and Engineering, Nanjing Tech University, 30 South Puzhu Road, Nanjing 211816, China*

[e] *Jiangsu Collaborative Innovation Centre for Advanced Inorganic Function Composites, Nanjing Tech University, Nanjing 211816, China*

[f] *Department of Building and Real Estate, The Hong Kong Polytechnic University, Hung Hom, Kowloon 999077, Hong Kong, China*

[g] *School of Energy and Power, Jiangsu University of Science and Technology, Zhenjiang 212100, China*

[h] *WA School of Mines: Minerals, Energy and Chemical Engineering, Curtin University, Perth, Western Australia 6845, Australia. E-mail: shaozp@njtech.edu.cn*

† Electronic supplementary information (ESI) available. See DOI: https://doi.org/10.1039/d3ee02695g

‡ These authors contributed equally to this work.

conversion and storage pathways thus become urgent and critical research topics.[1] In recent years, the utilization of renewable solar, wind and hydroelectric energy *via* power plants has helped relieve the pressure of the above crises to a certain extent. However, the intermittence of these resources and the saturation of the power grids (at most ~15% external input) hinder the development of this route.[2,3] Utilizing the excess electricity converted from renewable sources to synthesize C/N/O/H-containing chemicals through an electrolysis roadmap can overcome this limitation.[4] For all the C/N/O/H-containing chemicals, hydrogen is an ingredient that produces important basic chemicals, such as ammonia, methanol and hydrochloric acid; additionally, hydrogen is an ideal energy carrier for the carbon-neutral plan and net-zero pathway due to its high calorific value (~282 kJ mol^{-1}), zero-carbon feature and environment-friendly merit.[2,5]

According to the analysis of global total final energy consumption by the International Energy Agency (IEA),[6] the proportion of hydrogen energy in the total final energy consumption should increase to ~2% and ~10% in 2030 and 2050, respectively, to realize the net-zero plan, along with the greatly decreasing consumption levels of nonrenewable fossil fuels (Fig. 1a). In addition, the total final energy consumption levels of renewables should increase by ~0.51% and ~7.41% in 2030 and 2050 compared with that in 2020, respectively.[6] The increased demand for renewables promotes electricity consumption, increasing from ~19.13% in 2020 to ~26.28% in 2030 and to ~49.23%[6] in 2050 (Fig. 1a). Notably, intermittent renewables can be transformed into electricity through power stations for grids, while excess electricity can be used to produce hydrogen *via* electrolysis; the effective conversion between hydrogen and electricity can be realized by fuel cells and electrolysers.[2,7] Therefore, hydrogen should play a critical and indispensable role in future long-term energy systems.

Then, insights into the trends of hydrogen demand and usage in living and production are provided here. As shown in Fig. 1b, the global hydrogen demand increased sharply from ~59 Mt in 2000 to ~74 Mt in 2010 and then to ~88 Mt in 2020.[6] These demands in 2030 and 2050 should increase to ~2.4 (~211 Mt) and ~6.0 times (~528 Mt) the demand in 2020, respectively,[6] demonstrating the importance of hydrogen in sustainable development. Regarding hydrogen utilization, hydrogen was mainly used in refining and industrial processes before 2020, and it will be increasingly and widely applied in transport, power, NH_3 fuel, synfuels, buildings and grid injection in the future (Fig. 1b).[6] It has been estimated that USD 7–8 trillion investment is required *via* the hydrogen-value chains by 2050, creating USD ~3 trillion revenues through the hydrogen economy.[8] Hence, hydrogen is in high demand, and it should be widely used throughout society.

Zero-carbon hydrogen plays a crucial role in CO_2 emission reduction. To realize the carbon neutral plan and net-zero pathway, detailed requirements for CO_2 emission reduction are proposed in various fields, including electricity, heat, industry, transportation, and buildings from 2020 to 2050 (Fig. 1c).[5] To accomplish these targets, the IEA notes that ~4.3 trillion USD should be invested in 2030, with the enlarged scale of low-carbon hydrogen and electrolysers in 2030 and 2045.[5] Specifically, ~150 Mt and ~435 Mt low-carbon hydrogen should be used in 2030 and 2045, respectively, while ~850 GW and ~3000 GW electrolysers should be in operation in 2030 and 2045, respectively.[5]

Then, producing sufficient hydrogen energy is the first key step. According to the different production modes, hydrogen can be divided into grey, blue and green hydrogen modes. As illustrated in the top of Fig. 1d, grey hydrogen is prepared by either reforming or gasifying coal, oil or natural gas.[9] Because of the high maturity and low cost (1–2 USD kg^{-1}, as revealed in Fig. 1e), grey hydrogen accounts for ~95% of all produced hydrogen resources.[10] However, impure grey hydrogen needs further complicated purification for usage, and ~10 kg CO_2 is simultaneously generated when producing 1 kg of grey hydrogen;[9] this generation strongly calls for sustainable low-carbon hydrogen modes. Blue hydrogen comes from steam methane reforming or gasification, and carbon capture and storage (CCS) technologies are applied (Fig. 1d, middle).[9] The captured CO_2 is injected into the deep porous rock layers for long-term storage under high pressure conditions.[9] Although blue hydrogen can meet the CO_2 emission requirements in most regions, nonrenewable fossil fuels must continue to be consumed; through this necessary consumption, 0.5–6 kg CO_2 should be emitted to produce 1 kg of blue hydrogen.[9] Moreover, the application of CCS technologies is rather strict and unsuitable in many areas.[9] Overall, the blue hydrogen mode is a transitional stage in the roadmap of long-term hydrogen production.
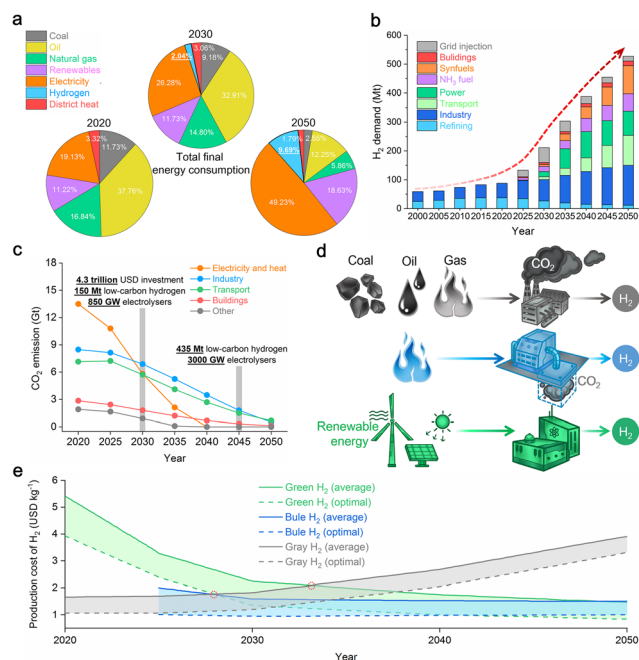

Fig. 1 Future of hydrogen energy. (a) Global total final energy consumption in 2020, 2030 and 2050. (b) Global hydrogen demand from 2000 to 2050. (c) CO_2 emissions from 2020 to 2050 under the net-zero pathway. (d) Schematic diagrams to produce grey hydrogen, blue hydrogen and green hydrogen. (e) Production cost for grey hydrogen, blue hydrogen and green hydrogen from 2020 to 2050, where the solid lines are the average costs, and the dashed lines are the optimal costs.

This journal is © The Royal Society of Chemistry 2023

Energy Environ. Sci., 2023, **16**, 4926–4943 | **4927**

Through electrochemical water splitting, the green hydrogen mode can use the electricity converted from solar, wind and hydropower sources for sustainable hydrogen production (Fig. 1d, bottom).[2] This route is regarded as the ideal method for hydrogen production in the future due to its multiple input resources (water and renewable electricity), zero carbon emissions, environmental friendliness and high hydrogen purity.[7] Additionally, the green hydrogen mode can solve the intermittence of renewable resources and the saturation of power grids. Based on the prediction of the Hydrogen Council and International Renewable Energy Agency (IRENA), ~30% of grey hydrogen will be replaced by green hydrogen in 2030[8] despite the recent proportion of green hydrogen being ~4% of all produced hydrogen sources.[3] The biggest obstruction to the green hydrogen mode is its high cost, which is still 4–5 times that for grey hydrogen (Fig. 1e).[10] With the development of renewable energy technologies and the introduction of revenue policies for CO_2 emissions, the cost of green hydrogen should be lower than that of grey hydrogen between 2028 and 2034 (Fig. 1e).[10] This indicates that the green hydrogen mode with the lowest future cost of ~1 USD kg^{-1} H_2 should gradually replace the grey hydrogen mode to realize the carbon neutral and net-zero plans.

2. Technologies for green hydrogen production

In addition to the green hydrogen produced by electrolysis, other routes utilizing renewable resources include photocatalysis, the solar thermochemical water-splitting cycle, photovoltaic electrolysis, supercritical water gasification of biomass and combined dark fermentation and anaerobic digestion.[3] The maturity of these technologies is quite different.[3] Compared with other hydrogen production pathways, electrochemical water splitting is relatively mature, and its modular feature is beneficial for large-scale hydrogen production at the present or near-future stage.[3] Herein, we focus on representative electrolysis technologies, demonstrate their respective advantages and disadvantages, and note their directions in the future. In addition, the promising technologies of photocatalysis, the solar thermochemical water-splitting cycle and photovoltaic electrolysis are briefly discussed.

In 1800, Nicholson and Carlisle found the phenomenon of electrochemical water splitting.[11] 100 MW plants were successfully built worldwide in the 1920s,[11] and the commercialization of water electrolysis began. Water electrolysis splits H_2O molecules into H_2 on the cathode (hydrogen evolution reaction (HER)) and O_2 on the anode (oxygen evolution reaction (OER)) under the function of direct currents (Fig. 2a–c). The components of electrochemical water splitting include the electrolyser, electrolyte, anode, cathode, separator, porous transport layer and bipolar plate. According to the different separators and electrolytes, five typical water electrolysis technologies can be included: alkaline water electrolyser (AWE), anion exchange membrane electrolyser (AEME), proton exchange membrane electrolyser (PEME), solid oxide electrolysis cell (SOEC) and
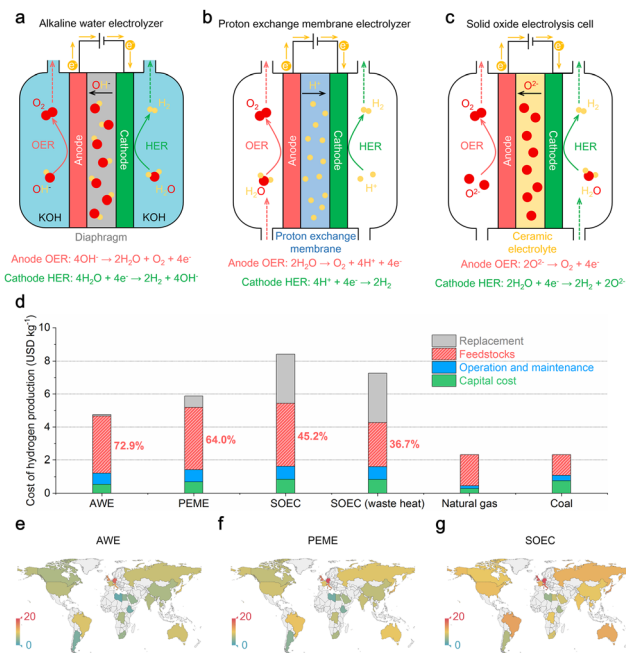

Fig. 2 Technologies of green hydrogen production. Schematic diagrams for (a) AWE, (b) PEME and (c) SOEC. (d) Specific hydrogen production costs of AWE, PEME, SOEC (without and with waste heat) and grey hydrogen (from natural gas and coal). Regional hydrogen production cost (USD kg^{-1} H_2) for (e) AWE, (f) PEME and (g) SOEC, where the grey parts are not calculated due to the lack of data.

protonic ceramic electrolysis cell (PCEC). Based on the operating temperatures, water electrolysis can be divided into low-temperature water splitting (<90 °C; AWE, AEME and PEME) and high-temperature water splitting (>300 °C; SOEC and PCEC). Concerning the maturity of commercialization, AWE and PEME technologies are commercialized, while AEME, SOEC and PCEC are still immature at the laboratory scale.[3]

As shown in Fig. 2a and Table S1, ESI,† AWE technology is relatively mature, with a present lifetime of 60 000 h and an expected lifetime of 100 000 h in 2050.[7] This technology works in 5–7 mol L^{-1} KOH solutions at 70–90 °C; thus, cost-effective nonprecious metal-based materials can be used as anodes and cathodes.[7] The produced H_2 and O_2 are physically separated by ZrO_2 stabilized with a polyphenylene sulfonic mesh,[7] where the OH^- and H_2O species can permeate through this porous diaphragm for electrochemical reactions. For other operating parameters, the present load range, current density and voltage efficiency of the AWE are 15–100%, 0.2–0.8 A cm^{-2} and 50–68%, respectively, which should be improved to 5–300%, >2.0 A cm^{-2} and >70% in 2050, respectively.[7] To date, the cold start to nominal load takes a long time (<50 min), but it should be shortened to <30 min in 2050.[7] To invariably maintain the pressure balance between the anode and cathode and avoid possible H_2/O_2 mixing, the electrolyser cannot quickly start or shut down. This makes AWE difficult to match with renewable resources with fluctuant features. Moreover, KOH solutions tend to react with CO_2 in air to form insoluble K_2CO_3 compounds, blocking the porous catalyst layers, hindering the transfer of

reactants/products, and reducing the overall hydrogen production efficiency.[7] To overcome the shortcomings of AWE, AEME was developed based on a solid electrolyte (divinylbenzene polymer support with KOH or $NaHCO_3$ (1 mol L^{-1})).[7] Benefiting from the relatively mild alkaline conditions and the application of a solid electrolyte, AEME can achieve larger current densities (0.2–2 A cm^{-2}), a faster cold start to nominal load (<20 min) and a higher voltage efficiency (52–67%) than AWE at the laboratory scale.[7] However, the recent laboratory-scale AEME membrane still shows poor chemical and mechanical stability and low conductivity, resulting in a poor lifetime (only ~5000 h).[7] Therefore, advancements in membrane optimization, electrode architecture and catalyst design are key for future commercialization.

Compared with alkaline AWEs and AEMEs, the solid electrolyte/separator (perfluoroacidsulfonic membrane) in acidic PEMEs is chemically and mechanically stable, enabling the effective transport of H^+ protons and realizing a relatively high cell pressure, wide load range, short time of cold start to nominal load, large current density, high voltage efficiency and long lifetime,[7] as presented in Fig. 2b and Table S1, ESI.† Hence, the flexibility and reactivity of PEME are higher than those of AWE and AEME, which can be effectively combined with renewable resources and yield profit from various electricity markets. In addition, PEME equipment is relatively simple and small (1500–2000 cm^2, much smaller than 10 000–30 000 cm^2 for commercial AWE), endowing PEME with flexible applications in large cities, temporary scenes and independent industrial zones.[7] However, due to the harsh conditions of high-purity deionized water at 50–80 °C, corrosion-resistant noble metals, Ti-based materials and protective coatings are necessary for the electrodes, porous transport layers and bipolar plates in PEMEs.[7] To date, although PEME has been increasingly commercialized, its system capital cost (700–1400 USD kW^{-1} in 2020 and <200 USD kW^{-1} in 2050) is still higher than that of AWE (500–1000 USD kW^{-1} in 2020 and <200 USD kW^{-1} in 2050).[7] Notably, PEME allows for a differential-pressure operation mode (reaching 70 bar at the HER side and atmospheric pressure at the OER side), which can effectively reduce the use of compressors to obtain compressed H_2 gas for subsequent H_2 storage and delivery, further lowering the related capital expenditure.[7] The biggest challenges are the fouling/degradation of PEME membranes induced by impurities in water and the expensive usage of noble metals,[7] making the development of efficient and cost-effective membranes and catalysts crucial in the future.

Relative to low-temperature water splitting (<90 °C), high-temperature water electrolysis (>300 °C) can further improve the whole hydrogen production efficiency due to the Arrhenius equation. Specifically, the voltage efficiency for the oxygen-conducting SOEC is 75–85% in 2020 and should be >85% in 2050 (Fig. 2c and Table S1, ESI†).[7] The present and future operating temperature, cell pressure and load range are displayed in Table S1, ESI.† Benefiting from advantageous high-temperature kinetics, SOECs can utilize noble-metal-free oxides as compositions.[7] Nonetheless, the high-temperature condition brings about problems of thermal compatibility and cycle

performance, leading to a limited lifetime of only <20 000 h in 2020 and 80 000 h in 2050.[7] Additionally, the cold start to nominal load for SOEC is overly slow (>600 min in 2020 and <300 min in 2050), and the costs for sealing and replacement remain high.[7] Therefore, SOECs are still developed with an electrode area of 200 cm^2 in the laboratory at the kW scale.[7] To reduce the operating temperature of SOEC, proton-conducting PCEC technology based on the solid electrolyte of Ba–Ce/Zr-containing perovskite oxides has been developed.[12] Compared with traditional SOEC, the PCEC cell can effectively transport many protons with small ionic radii in the proton-conducting electrolytes, contributing to its low transfer energy barrier, high conduction efficiency and reduced operation temperature at temperatures of 300–600 °C.[12] These features make the PCEC technology a highly promising next-generation technology for hydrogen production. However, the ceramic and rare materials used in SOECs and PCECs remain expensive, and the demand for stable heat resources still limits their long-term economic feasibility.[12] Moreover, certain issues must be solved for the commercialization of SOECs and PCECs in the future, *e.g.*, the sealing of the cells at high differential pressure and the degradation caused by additional contaminants from sealants, piping and interconnections.[7]

In addition to the above electrochemical water electrolysis triggered by electricity, renewable solar energy can be directly used for water splitting. In 1972, Akira Fujishima and Kenichi Honda[13] reported pioneering work on water photolysis on TiO_2, which is called the Honda–Fujishima effect and brings photocatalysis to the forefront of fundamental research in energy fields. According to the specific energy input, water photolysis can be divided into three categories: photocatalysis, solar thermochemical water-splitting cycle and photovoltaic electrolysis. Solar and solar-transformed thermal energies are the inputs of photocatalysis and the solar thermochemical water-splitting cycle, respectively, while coupled solar and electricity are applied in the photovoltaic electrolysis. Photocatalysis can directly split water into H_2 and O_2 on photocatalysts, and its system design is cost-effective and simple.[14] Recently, Domen *et al.*[14] used an Al-doped $SrTiO_3$ photocatalyst to build a 100 m^2 panel photocatalytic system with the function of autonomous H_2 recovery from gas products, which can be safely operated for several months. However, the maximum solar-to-hydrogen (STH) efficiency of photocatalysis is still limited to within 1%. Recently, Mi *et al.*[15] optimized the photocatalytic operation temperature on the InGaN photocatalyst (optimum temperature of ~70 °C) and realized an STH efficiency of 9.2%, overcoming the STH efficiency bottleneck of photocatalysis. The scholars found that this temperature-dependent strategy is applicable for scenarios using tap water, seawater or natural solar light. However, the STH efficiency (≥10%), photocatalytic stability (≥10 years) and gas separation efficiency of photocatalysis should be further enhanced to realize the proposed commercial cost target (≤USD 102 m^{-2}),[16] which calls for continuous advances in system, process, and material design optimization. The solar thermochemical water-splitting cycle can transform solar energy into thermal energy *via* solar

collectors to realize sequential high-temperature reduction $(2M_xO_y \rightarrow 2xM + yO_2)$ and water splitting on a metal oxide $(xM + yH_2O \rightarrow M_xO_y + yH_2)$ at hundreds or thousands of degrees.[17] Due to the separated steps of H_2 and O_2 production, gas separation is not an issue for this technology. Moreover, by simultaneously introducing CO_2 and H_2O to react with metal oxides, syngas products can be obtained $(M_xO_y + CO_2 \rightarrow M_xO_{y+1} + CO; M_xO_y + H_2O \rightarrow M_xO_{y+1} + H_2)$.[18,19] However, the STH efficiency and solar-to-syngas efficiency of the solar thermo-chemical water-splitting cycle are still low, at 15–30%[17] and 1–4%,[18,19] respectively. When coupling solar with electricity in photovoltaic electrolysis, an STH of 30% can be realized at the laboratory scale.[20] Overall, compared with electrochemical water electrolysis with much higher hydrogen production efficiency and stable operation, the above photocatalysis technologies will take more time to achieve further commercialization.

To further analyse the specific costs of green hydrogen production, we calculate the detailed costs for AWE, PEME, SOEC (without and with waste heat) and traditional hydrogen production from natural gas and coal (details in the Supplementary Note and Tables S2–S4, ESI†). As revealed in Fig. 2d, the present total hydrogen production cost follows the ordering of grey hydrogen (from natural gas and coal) < AWE < PEME < SOEC (waste heat) < SOEC, which mainly contains the costs of capital, operation, maintenance, feedstock and replacement. Notably, the major cost originates from the feedstocks: electricity consumption. Specifically, the electricity consumption levels in AWE, PEME, SOEC and SOEC (waste heat) account for ~72.9%, ~64.0%, ~45.2% and ~36.7% of respective total costs, respectively. Therefore, reducing the electricity consumption levels in green hydrogen technologies are key for their commercial development.[7]

Furthermore, to compare the total hydrogen production costs in different regions, we calculate the total hydrogen production costs of AWE, PEME and SOEC in representative areas worldwide based on the latest electricity prices (Table S5, ESI†).[21] As exhibited in Fig. 2e–g, the total hydrogen production cost in representative regions for SOEC is the highest, while that for AWE is the lowest. Notably, due to the differences in regional resources and electricity prices, the total production cost greatly varies among different areas, resulting in a very high hydrogen gap and in mismatching worldwide. The Hydrogen Council reported that this situation will be relieved by global hydrogen flows between areas with high demand and low supply and areas with low demand and high supply.[22] In 2050, China will become the largest hydrogen market, with 200 million tons of hydrogen demand; additionally, global hydrogen trade will continuously deepen, develop and grow, where 400 million tons of renewable low-carbon hydrogen and derivative resources will be inputted into hydrogen flows to solve the worldwide supply demand imbalance.[22]

Overall, the recent major cost of green hydrogen production comes from electricity consumption. As shown in Table S1, ESI,† designing and developing efficient and stable electrocatalysts to reduce electricity consumption has become quite important for optimizing the parameters of green hydrogen technologies.[7]

3. Catalyst design for hydrogen production

Water electrolysers for green hydrogen production contain HER on cathodes and OER on anodes, which can operate in acidic, alkaline, neutral, seawater or solid-state electrolytes.[23–26] The overall efficiency and stability of water electrolysers depend on HER and OER electrocatalysts. The prototypical state-of-the-art catalysts for the HER and OER are expensive and scarce; for example, Pt, Pd and Rh are scarce for the HER and RuO_2 and IrO_2 are scarce for the OER.[23,27] For acidic water splitting, the HER kinetics are fast $(2H^+ + 2e^- \rightarrow H_2)$, where noble metal-based Pt and its alloys[28] or nonprecious materials, such as MoS_2,[29,30] $NiMoN_x$,[31] $CoSe_2$,[32] Ni_2P,[33] Mo_2C,[34] MXenes[35] and C_3N_4,[36] can serve as promising candidates. However, the acidic OER is sluggish $(2H_2O \rightarrow O_2 + 4H^+ + 4e^-)$, and the catalysts are highly unstable;[37] optimized precious Ir/Ru-based materials are always required to achieve reasonable activity and stability.[38] Recently, some promising nonnoble metal-based electrocatalysts have been developed for the acidic OER, such as La- and Mn-codoped cobalt spinel,[39] Co_2MnO_4 spinel,[40] γ-MnO_2 oxide[41] and the Ba salt of a Co-phosphotungstate polyanion,[42] which still require further optimization and enhancement in activity and stability.[38] Compared with the harsh conditions of acidic water splitting, the stabilities of electrocatalysts for alkaline water electrolysis are enhanced, and many efficient catalyst families for alkaline OER have been developed, such as oxides, spinels, perovskites and hydroxides.[43–45] However, due to the interfacial water interactions with catalysts to form hydrogen protons $(2H_2O + 2e^- \rightarrow H_2 + 2OH^-)$, the alkaline HER is more sluggish than the acidic HER.[46,47] This is why designing and developing alternatives to enhance the stability in acid and facilitate the alkaline HER are highly sought after.[48–51] Compared with acidic and alkaline water electrolysis, neutral water splitting can address the issues of a corrosive working environment, expensive cation/anion exchange membranes, and anti-corrosive electrocatalysts, which can enable low-cost direct seawater electrolysis and bioupgraded chemical fuels.[24,52,53] However, the kinetics of neutral water splitting are relatively slow, calling for future advances in the development of efficient and stable catalysts.[24,52] Regarding direct seawater splitting, overcoming the competition of chlorine chemistry and the influences of other impurities (e.g., metal ions and bio-organisms) are key for the rational design of electrocatalysts.[25] Notably, indirect seawater electrolysis via seawater desalination, water vapour transport or hygroscopic electrolytes for electrochemical hydrogen production may solve the above issues in direct seawater splitting.[54–56] Benefitting from the thermodynamic effects, high-temperature solid-state SOEC and PCEC are more efficient than the abovementioned technologies for hydrogen production; however, the stability levels of electrocatalysts for SOEC and PCEC should be further increased.[26]

From the standpoints of material morphologies, macroscopic physiochemical properties, molecular-level structural information and electronic structural features, we discuss catalyst design principles and methodologies for green hydrogen

4930 | *Energy Environ. Sci.*, 2023, **16**, 4926–4943

This journal is © The Royal Society of Chemistry 2023

production. Moreover, insights into the effective screening of promising material candidates are given, aimed at reducing the time and cost required for catalyst design and development.

Concerning catalyst morphologies, nanotechnologies are widely applied to increase material surface areas and improve atomic utilization and catalysis performance. As illustrated on the left in Fig. 3a, with decreasing catalyst particle size, material active surface areas are enlarged and exposed to catalysis reactions, which is called the size effect.[57] Applying various nanotechnologies can effectively reduce catalyst particle size to exert a beneficial size effect. For noble-metal-based catalysts, nanotechnologies can effectively reduce the usage of precious metals, improve material atomic utilization and reduce material costs. The engineering of nanomaterials has developed rapidly in recent years from 3D nanoparticles (polyhedron, alloy and core–shell)/nanoframes to 2D nanosheets/nanofilms, to 1D nanorods/hollow nanorods and further to 0D nanodots/single atoms[4,57] (Fig. 3a, middle and right). Notably, 0D single atoms possess the smallest particle sizes and the highest atomic utilization levels to enhance the catalysis performance,

which has been promoted to the forefront of green hydrogen production in recent decades.[57] However, cost-effective and scalable nanomaterials should be further developed for future commercialization. Concerning the element choice, introducing multiple elements into electrocatalysts can exert beneficial synergistic effects (*e.g.*, Ni–Fe and Co–Fe couples for efficient OER) or high-entropy effects (*i.e.*, sluggish diffusion effect, severe lattice-distortion effect and cocktail effect) to reduce the overpotentials and Tafel slopes for the OER and HER.[58–61]

Regarding macroscopic physiochemical properties, the material liquid/gas–solid contact angle, magnetism and electron-transfer capability are often optimized to improve the catalytic efficiency. For the contact angle, when the liquid/gas–solid contact angle is $<90°$, materials show hydrophilicity/aerophilicity,[62] while when the contact angle is $>90°$, catalysts exhibit hydrophobic/aerophobic features[62] (Fig. 3b(I)). The hydrophilic/aerophilic catalyst surface can help adsorb liquid/gas reactants,[62] while the aerophobic feature can desorb H_2/O_2 products in a timely manner to avoid H_2/O_2 coverage on material active sites; this may enhance the reaction kinetics.[62] Actually, the contact angle is determined by the triple-phase tensions (gas, liquid and solid), following the Young equation.[63] The tensions are closely correlated with catalyst surface properties,[63] making material surface tuning an effective method for moderating the contact angle and optimizing the catalysis efficiency. For material magnetism properties, ferromagnetism (FM) is defined when the magnetic moments of two adjacent atoms are parallel, those for antiferromagnetism (AFM) are anti-parallel, and those for paramagnetism (PM) show no orderings (Fig. 3b(II)). Reportedly, FM and coupled material systems can exhibit the effects of spin polarization, spin exchange and spin pinning to promote the adsorption/desorption characteristics of intermediates and enhance electron transport in electrochemical water splitting.[64,65] By applying external magnetic fields, these favourable effects can be enhanced on FM-containing materials to further accelerate catalysis.[64,65] Thus, modulating material magnetism properties is helpful for optimizing catalysis and improving the water electrolysis performance. For electron transfer, the high electrical conductivity of catalysts can boost the electron transport steps and electrochemical kinetics in water splitting. Notably, a unique electronic double exchange phenomenon exists in some systems.[66] The double exchange mechanism is that local spin remains when electrons hop between ions with different oxidation states.[66] As demonstrated in Fig. 3b(III), the Mn^{3+}–O–Mn^{4+} configuration follows the typical double exchange mechanism.[66] If one electron on the O 2p orbital transfers to the e_g orbital of the Mn^{4+} ion, the vacant O 2p orbital can accept another electron from the adjacent Mn^{3+} ion, remaining in the Mn^{4+}–O–Mn^{3+} configuration without spin variations. A similar phenomenon exists in the superexchange mechanism, *e.g.*, the Ni^{3+}–O–Mn^{3+} configuration.[67] These delocalized electron behaviours can help accelerate electron transfer and improve the performance in water electrolysis.[67]

Material structural properties offer molecular-level active and stable sites, which are significant for the activity and stability of water electrolysis. The smallest structural units,
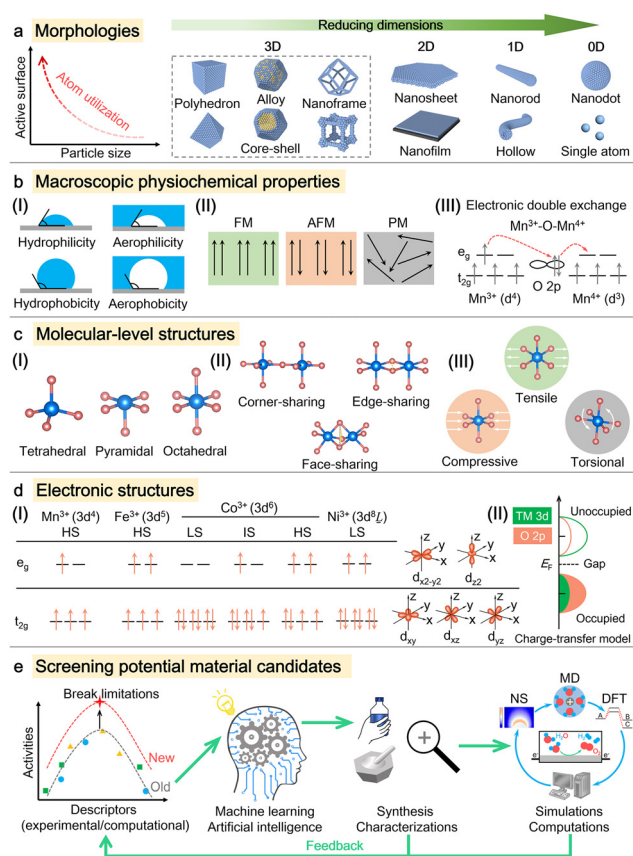

Fig. 3 Methodologies of the rational catalyst design and screening pathways. (a) Size effect and different electrocatalyst morphologies. (b) Macroscopic physiochemical properties of electrocatalysts including (I) liquid/gas–solid contact angle, (II) magnetism and (III) electron transfer. (c) Material molecular-level structural information including (I) coordination, (II) connected motif and (III) strain. (d) Electronic structural features of (I) 3d^{3+} ions with different spin states and (II) the charge-transfer model. (e) Workflow diagram of screening potential material candidates.

This journal is © The Royal Society of Chemistry 2023

Energy Environ. Sci., 2023, **16**, 4926–4943 | **4931**

including tetrahedral, pyramidal and octahedral units (Fig. 3c(I)), can exert different coordination chemical effects to adsorb/desorb the reactants, intermediates and products, further affecting the catalysis performance.[68–70] The connection between the smallest structural units mainly includes the corner-sharing, edge-sharing and face-sharing configurations.[71–73] As exhibited in Fig. 3c(II), by taking the octahedral transition metal (TM)–O configuration as an example, we can determine that one TM ion can connect with the adjacent TM ion *via* one, two or three couples of TM–O–TM combined bonds; these configurations are defined as the corner-sharing, edge-sharing and face-sharing motifs, respectively.[71–73] Different connected motifs in local structures show the different states of active and stable sites. From the corner-sharing structure to the edge-sharing unit and to the face-sharing motif, the distance between adjacent TM ions shortens from ~ 3.9 Å to ~ 2.9 Å and to ~ 2.4 Å.[71–73] The close TM–TM distance may create short reaction pathways for reactants and intermediates, contributing to the enhancement in reaction efficiency.[72,74] Moreover, the increased number of TM–O–TM combined bonds from corner-sharing to edge-sharing and to face-sharing units can help stabilize the structure, which may improve the durability of water electrolysis.[72–74] Therefore, understanding material molecular-level structures is important for rational catalyst design. Strain is induced by material structures, and a strain tuning strategy is effective for optimizing the water electrolysis performance.[75] As shown in Fig. 3c(III), the structural strain mainly contains compressive, tensile and torsional strains.[75] Optimal strain can effectively moderate the adsorption/desorption capabilities of electrocatalysts to improve the performance.[75]

Under electrochemical water electrolysis conditions, oxidation and reduction processes are triggered, and these procedures are accompanied by variations in material electronic structural properties, including valence, spin and orbital states.[76] Among numerous TM elements, 4d and 5d TM ions usually exhibit a low-spin (LS) state due to their strong crystal fields,[77] while 3d TM ions possess abundant electronic structures.[78] By taking trivalent octahedral 3d TM ions as an example (Fig. 3d(I)), we can find that 3d TM orbitals split into two high-energy e_g orbitals ($d_{x^2-y^2}$ and d_{z^2}) and three low-energy t_{2g} orbitals (d_{xy}, d_{xz} and d_{yz}); Mn^{3+} and Fe^{3+} are in the high-spin (HS) state, Ni^{3+} is LS and Co^{3+} can be either LS, intermediate spin (IS) or HS.[78,79] In recent decades, material e_g occupancy,[80] covalence,[81] band centre,[82] charge transfer energy[83] and valence state[84] have been successfully exploited as activity descriptors to guide material design for water electrolysis. Actually, the underlying correlations among these electronic structural parameters can be successfully demonstrated by the physical charge transfer model.[85,86] By taking 3d TM oxides as an example, the unoccupied TM 3d and O 2p orbitals (*i.e.*, conduction band) are above the Fermi level (E_F), while the occupied TM 3d and O 2p orbitals (*i.e.*, valence band) lie below E_F, where unoccupied and occupied orbitals are separated by the band gap (*i.e.*, forbidden band),[68,86] as illustrated in Fig. 3d(II). With the increase in 3d TM valence, the mixing of TM 3d-O 2p orbitals is enhanced (TM 3d-O 2p covalence strengthens), along with the shift of unoccupied and occupied orbitals to E_F (the orbital band centres move towards E_F) and the reduced charge transfer energy value (energy difference between the TM 3d band and O 2p band).[86,87] Notably, the overlapping characteristics of unoccupied and occupied orbitals for high-valence Co^{4+}, Fe^{4+}, Cu^{3+} and Ni^{3+} ions are strong, eliminating the band gap.[68,88] This can endow the above ions with metal-like TM sites and active O 2p orbitals to help promote the adsorption/desorption of H^+ protons in the HER[68] and trigger possible lattice oxygen participation in the OER,[89] respectively. In addition, for TM 3d ions with the same valence, the TM 3d–O 2p covalence decreases from Cu^{n+} to Ni^{n+}, Co^{n+}, Fe^{n+} and Mn^{n+}, while the band centre shifts towards E_F from Mn^{n+} to Cu^{n+} with decreasing charge transfer energy values.[86,87] These important conclusions may be helpful for the rational design of material electronic structural properties to optimize the performance of water electrolysis.

Finally, to effectively screen and exploit active and robust electrocatalysts for green hydrogen production, we show rational and instrumental pathways and methodologies for guidance. As described in Fig. 3e, first, data are collected from various experimental and computational material physico-chemical parameters and their corresponding performance characteristics from databases or literature as the input into the artificial intelligence machine learning algorithm. Machine learning can reveal the relationships between various material physicochemical parameters and material performance to demonstrate the structure–activity relationships and determine promising new catalysts. Then, predicted material candidates are experimentally synthesized and characterized *via* systematic *operando*, *in situ* and *ex situ* characterizations to offer detailed insights into catalyst morphologies, macroscopic physiochemical properties, molecular-level structural information, electronic structural features and adsorption capabilities. The methodologies for designing of experiments[90] and statistical analyses[91] are powerful to help understand the underlying structure–activity relationships in this step. These results and conclusions should offer sufficient and reliable information for computational calculations and simulations. From numerical simulations (NSs) to molecular dynamics (MDs) and to density functional theory (DFT) calculations, we can theoretically reveal and understand the possible catalysis mechanisms from the macroscopic to the microscopic level. The newly extracted experimental/computational parameters and findings can supplement the old database or even overcome the prior structure–activity limitations to build new relationships and descriptor systems for future material design and development. Through continuous screening, feedback and updates, further efficient and robust electrocatalysts are effectively developed, promoting the future commercialization of green hydrogen technologies. To date, from a theoretical standpoint, descriptor-based analyses are mostly applied based on the adsorption energies of the reaction intermediates.[28,92–94] In addition, numerous other descriptors have been developed, such as the orbital e_g occupancy,[80] band centre,[82,95–97] charge transfer energy,[83,98] valence state,[84] outer electrons,[99] ionic electronegativity,[100] bond strength,[101] coordination number,[102] strain,[103] tolerance

4932 | *Energy Environ. Sci.*, 2023, **16**, 4926–4943

This journal is © The Royal Society of Chemistry 2023

factor,[104] Curie/Néel temperature,[105] enthalpy,[106] bulk formation energy,[107] electrocatalytic symmetry/asymmetry,[108,109] and multiphysicochemical material properties.[110] Although descriptor-oriented machine learning has been utilized for screening HER and OER catalysts, the lack of sufficient and reliable datasets and methods still limits their wide applicability in water electrolysis.[111,112]

4. Hydrogen storage

Storing hydrogen efficiently, safely, and economically is important for hydrogen delivery and onboard hydrogen storage processes. Physical-based hydrogen storage is the most mature method, in which 350 and 700 bar nominal working pressure compressed gas tanks are widely used for onboard automotive utilization (compressed gas in Fig. 4a).[113] The aboriginal gas tanks are made of aluminium or steel (type I), which can store hydrogen at a maximum pressure of 300 bar.[114] Certain
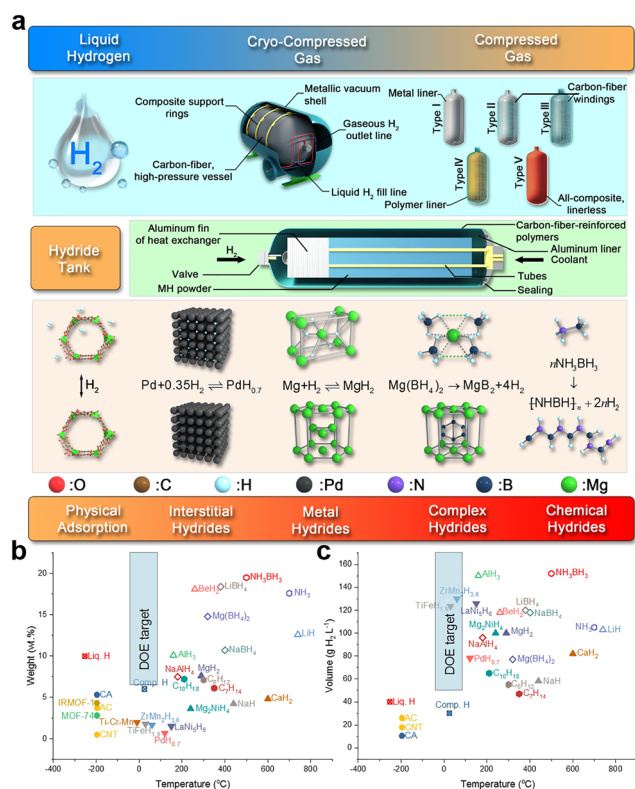

Fig. 4 Hydrogen storage technologies. (a) Three physical-based hydrogen storage methods (above), a hydride tank (middle), and five representative material-based hydrogen storage techniques (bottom), where the ordering is based on their operation temperatures. (b) Gravimetric capacities of typical hydrogen storage methods/materials. (c) Volumetric capacities of typical hydrogen storage methods/materials, where the hydrogen storage capacities of physisorption-based materials were measured at 77 K for comparison. The shapes of labels in (b) and (c) represent different kinds of hydrogen storage methods/materials. Squares: physical methods; dots: physical adsorption; inverted triangles: interstitial hydrides; triangles: metal hydrides; diamonds: complex hydrides; and hexagons: chemical hydrides. The filled labels indicate good reversibility, and hollow labels indicate the opposite. DOE targets are marked in light blue rectangles.

additions, such as carbon-fibre windings (for type II and type III) and polymer liners (for type IV), which can strengthen the physical qualities, have been adopted to increase the hydrogen storage pressure capacity. Type IV hydrogen tanks, which have composite material-based inner liners and are encased in an outer wrapping made of carbon fibre, can store hydrogen at a maximum pressure of 700 bar; the reported gravimetric capacity is 5.7 wt%.[115] Although type IV hydrogen tanks have been widely used in fuel cell vehicles, the system cost can reach approximately USD 500 kg^{-1} H$_2$, which is almost twice the ultimate target (USD 266 kg^{-1} H$_2$) of the Department of Energy (DOE).[116] Moreover, the type V tanks are composed of lightweight composites that are integrated without a liner, thereby realizing a 20% reduction in weight. However, these tanks can only be used in low-pressure ranges (operation pressure: 14 bar and proof pressure: 69 bar), and they are still being researched.[117]

Hydrogen can be stored in liquid form. Low-temperature liquid hydrogen has a high volumetric storage capacity of 30–50 g H$_2$ L^{-1} depending on the storage vessels[118] (liquid hydrogen in Fig. 4a). The precooled Claude method and the helium refrigerated system are commonly used during the hydrogen liquefaction. The main challenges for liquid hydrogen in practical processes are reducing the total cost of cooling liquefaction and maintaining low temperatures to prevent boil-off. To date, liquid hydrogen is not considered the best method for automotive hydrogen storage. However, liquid hydrogen is an ideal energy source for applications requiring high energy density and gas purity levels, such as spaceflight projects.

Cryo-compressed hydrogen storage systems that combine the two technologies discussed above appeared early in this century (cryo-compressed gas in Fig. 4a). The implemented pressure and temperature levels depend on the specific usage scenario. Regarding onboard usage, a high pressure and low temperature, i.e., 500 bar and 80 K, are required for high hydrogen density (75 g H$_2$ L^{-1}) applications.[119] Loose storage conditions are relatively suitable for hydrogen delivery considering the total cost, especially regarding the prevention of heat leakage during prolonged storage. The high-pressure insulated vessel can decrease liquid hydrogen boil-off losses, thereby extending the storage period. Relative to type IV hydrogen tanks, the consumption levels of carbon fibre composites and the system costs of cryo-compressed hydrogen storage systems are decreased by 46% and 21%, respectively.[120] According to the gravimetric and volumetric targets proposed by DOE, cryo-compressed hydrogen storage is a potential candidate for automotive applications. Improving infrastructure availability and reducing its cost are the key focuses of the next steps.

Although physical-based hydrogen storage strategies are valuable and important, their hydrogen capacity and energy density, remain limited. Alternatively, increasing efforts have been devoted to material-based hydrogen storage methods, achieving a relatively high hydrogen storage capacity under moderate pressure and temperature conditions and resulting in improved safety and reduced consumption levels for H$_2$ storage and transportation applications. Hydrogen storage

materials (HSMs) can store hydrogen in two different manners: physisorption and chemisorption.[121] For physisorption, the hydrogen storage capacities positively relate to the specific surface areas of the materials (physical adsorption in Fig. 4a). Porous materials, such as metal–organic frameworks (MOFs), covalent organic frameworks (COFs), zeolites, and carbon materials are ideal candidates for physisorption HSMs.[122] Hydrogen molecules gather on the surfaces of HSMs through van der Waals forces with low binding energies (4–10 kJ mol^{-1} H$_2$), leading to superior hydrogen adsorption/desorption kinetics.[123] However, the low binding energy makes it difficult to trap hydrogen molecules at moderate temperatures and pressures. The hydrogen storage capacities of these materials depend greatly on the operating conditions. For example, the reported gravimetric capacity of carbon aerogel decreases from 5.3 wt% to 0.9 wt% when the temperature increases from 77 K to 298 K.[124] Introducing hydrogen affinity metal ions/nanoparticles into porous materials can improve the binding energy, making it possible to store hydrogen via physical adsorption at room temperature. Another challenge is to screen high-performance candidates for physisorption because there are over one million reported MOFs/COFs/zeolites.[125] Parts of the datasets are first simulated by the grand canonical Monte Carlo (GCMC) method for obtaining the hydrogen storage properties. Machine learning models are then utilized to fit the chemical/topological/crystallographic features and the corresponding calculated hydrogen storage properties of the porous materials. Finally, the accuracy and robustness characteristics are validated to obtain the best model. The obtained machine learning model can accurately predict the hydrogen storage properties with less than 0.02% of the computational resources of GCMC.[126] This technology can significantly shorten the screening process. Furthermore, machine learning models can predict the hydrogen storage performance levels of chemisorption HSMs once suitable features and sufficient training data are available.

Chemisorbed HSMs can be classified into several subclasses, including interstitial (Fig. 4a PdH$_{0.7}$), metal (Fig. 4a MgH$_2$), complex (Fig. 4a Mg(BH$_4$)$_2$), and chemical (Fig. 4a nNH$_3$BH$_3$) hydrides. Hydrogen absorption/desorption is accompanied by the dissociation/recombination of hydrogen molecules, during which a high energy barrier must be overcome. Thus, the operating temperatures of the chemisorbed HSMs are significantly higher than those of the physisorbed HSMs. Interstitial, metal, and complex hydrides are all metal-based HSMs, indicating that they possess similar features. First, most of the hydrogen adsorption/desorption reactions of these HSMs are gas–solid reactions; thus, the kinetics are influenced by the solid phase mass transfer and surface reaction processes. Consequently, catalysing and nanoscaling HSMs are essential for improving the kinetics. Second, these hydrides are easily passivated by gaseous contaminants, such as O$_2$, H$_2$O, and CO$_2$ in the air, sharply decreasing the hydrogen reactivity level. Certain techniques, such as surface modification and nanoconfinement, are conducted to alleviate kinetic degradation.[127–129] Finally, an efficient vessel (hydride tank in Fig. 4a) to store the hydride powder is a vital part of practical utilization. A heat transfer system and a hydrogen flux control system should be included in a typical hydride tank, achieving a much higher volumetric capacity than that of a gas tank at room temperature.[130] Recently, hydride tanks have been designed to be combined with pressurized hydrogen (<30 MPa) to form a new type of composite tank: a high-pressure metal hydride (HPMH) tank.[131] In an HPMH tank, compact hydrogen storage is achieved via both material-based and physical-based methods: hydrogen is first released from the pressurized gas, followed by the desorption of solid-state metal hydrides. This strategy is highly appropriate for metal hydrides with high-pressure plateaus, such as LaNi$_5$.

Despite the similarities, the gravimetric capacity and reversibility characteristics of the three types of hydrides vary greatly. Interstitial hydrides generally show excellent reversibility near room temperature because of the weak metallic bonds between hydrogen and metal atoms. However, the gravimetric hydrogen densities of these hydrides are low (<2 wt%), and most of them are nonstoichiometric because the hydrogen atoms occupy the interstitial sites of metal crystals.[132] Distinguished from interstitial hydrides, metal hydrides have specific stoichiometric formulas and different crystal structures from their counterpart metals. Usually, metal hydrides exhibit higher gravimetric capacity than interstitial hydrides (Fig. 4b). However, the dehydrogenation temperatures of the metal hydrides are relatively high (>200 °C) because the chemical bonds in these hydrides are commonly ionic or covalent, which are more difficult to break than interstitial bonds.[133] For example, MgH$_2$ can reversibly store 7.6 wt% hydrogen, but its desorption enthalpy reaches 74 kJ mol^{-1} H$_2$, resulting in a high operating temperature of over 300 °C under atmospheric conditions. Complex hydrides are metal salts containing a metal cation centre and surrounding hydride anions, such as alanates ([AlH$_4$]$^-$), amides ([NH$_2$]$^-$), imides ([NH$_4$]$^-$), and borohydrides ([BH$_4$]$^-$).[134] These hydrides possess extremely high theoretical hydrogen storage capacities. For example, the gravimetric capacity of LiBH$_4$ is 18 wt%, which is 11 times that of the commercially used hydride-forming alloy LaNi$_5$. However, the poor reversibility, impure gaseous products, and high decomposition temperature have hindered their onboard utilization. Another possible application scenario of complex hydrides is as a disposable hydrogen source by hydrolysis reaction, providing high-purity hydrogen for proton-exchange membrane fuel cells (PEMFCs) directly.[135]

Chemical hydrides, including organic and inorganic hydrides, are promising candidates for hydrogen carriers due to their high gravimetry and easy handling. For example, ammonia borane (nNH$_3$BH$_3$) is one of the highest-capacity hydrogen storage materials (19.6 wt% in gravimetric capacity and 151 g H$_2$ L^{-1} in volumetric capacity). Another advantage is the high compatibility with the existing energy infrastructures.[136] Most chemical hydrides can be transported in gaseous or liquid form, indicating that the existing pipelines for natural gas or oil can be updated to satisfy the requirements of chemical hydride delivery. Noble metal-based catalysts are always necessary to improve the poor dehydrogenation kinetics.[137] The reversibility characteristics of chemical hydrides are far from satisfactory since the reactions are thermodynamically difficult, especially for inorganic hydrides.

Moreover, the large enthalpies of the organic hydrides determine a high dehydrogenation temperature. Incorporation with other atoms, such as boron or nitrogen, can reduce the dehydrogenation enthalpy to a certain extent.[138]

Although various methods for hydrogen storage have been developed, few can fulfil all the requirements of onboard hydrogen storage raised by the DOE considering critical technical specifications (Fig. 4b and c and Table S6, ESI†).[139] Physical-based methods, especially compressed hydrogen, are compromised in the present stage. Contrary to physical-based methods, material-based methods are attracting further attention, and they are regarded as final solutions due to their environmental, economic, technical, and social advantages.[140] To achieve this feat, specific technical barriers should be overcome. First, the overall performance characteristics of the HSMs should be improved. According to the above descriptions, most chemisorption-based HSMs show high operation temperatures over 200 °C, making them unsuitable for onboard utilization. This issue can be modified from the aspect of kinetics and thermodynamics. Certain strategies, such as catalysing and nanosizing, can reduce the energy barriers of dehydrogenation reactions.[141–143] Additionally, multialloying by atomic doping or element substitution and compositing can change the enthalpy levels of the reactions. Second, system costs should be further reduced, including capital, finance, operation, maintenance, repair and replacement costs. For example, by adjusting the electronic structures, nonnoble metal-based catalysts probably perform better than noble metal-based catalysts. Finally, the coupling between hydrogen storage and consumption systems should be further developed. A typical case is hydrogen heat coupling between hydride tanks and solid oxide fuel cells (SOFCs). For example, the wasted heat from SOFC can be reused to facilitate the dehydrogenation of metal hydrides in metal tanks, thereby improving the system energy efficiency.

5. Hydrogen delivery

Hydrogen delivery is a necessary process in the future hydrogen society, considering that significant geographical separation generally exists between centralized hydrogen production facilities and end use. The potential delivery routes are closely related to the detailed scenarios, *e.g.*, the technical maturity of various hydrogen storage technologies and the state of hydrogen at end use. (Fig. 5a). However, specific technical challenges still exist, and reducing the economic cost is the most critical issue for hydrogen delivery.[144] The DOE has proposed that the ultimate goal of the total hydrogen delivery cost should be less than half the cost of hydrogen end-use sales (USD 4 kg^{-1} H$_2$), namely, less than USD 2 kg^{-1} H$_2$.[144] In this section, we discuss the various modes of hydrogen delivery desirable for the future hydrogen society and the key technical issues to be addressed. Moreover, we propose designs of hydrogen production and delivery routes based on some hypothetical scenarios to meet the end-use cost target of hydrogen by our original techno-economic analysis.

In the future hydrogen society, the delivery process generally consists of three levels: transmission, distribution, and dispensing. Transmission is the large-scale and long-distance transport of hydrogen or hydrogen carriers from central hydrogen production facilities in renewable-rich regions to regional transfer terminals. Then, distribution sends hydrogen to centralized hydrogen use sites and hydrogen refuelling stations; the fuel-cell vehicle (FCV) is a very important scenario for hydrogen use. Finally, dispensing delivers hydrogen to end users in different locations through refuelling stations or city pipeline networks. For the actual delivery route design, multi-level transport by combining different delivery modes should be appropriately planned based on volume, distance, geographic conditions, circulating period, policies and safety to reduce the total delivery cost (Fig. 5a). Thus, delivery pathway design and optimization are needed to evaluate the costs and other impacts of specific scenarios.[145] In addition, on-site hydrogen storage can be implemented in renewable-rich regions without hydrogen delivery by combining the hydrogen production with water electrolysis, hydrogen storage, and fuel cells power generation; furthermore, this system can convert highly volatile renewable electricity to grid-connected
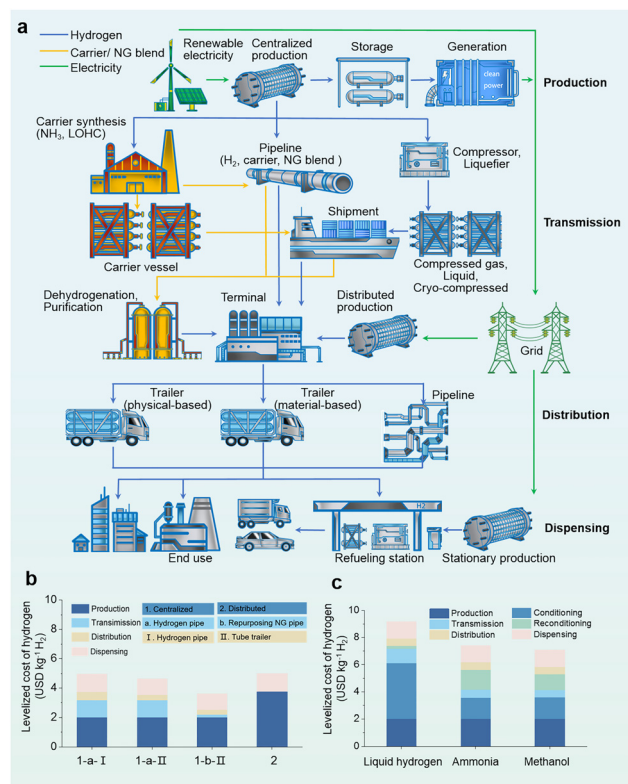

Fig. 5 Routes and economic analyses of hydrogen from source to end. (a) Promising hydrogen production and delivery routes, where the delivery consists of transmission, distribution, and dispensing. The routes of on-site hydrogen energy storage and distributed hydrogen production are considered. The calculated total levelized costs of hydrogen at the refuelling station for scenarios of hydrogen delivery (b) from Gansu Province to Shanghai, China (continental transport) and (c) from Australia to Japan (intercontinental transport).

electricity. Due to a high capacity and long storage period, this approach can compete with battery energy storage.[146]

The transportation of pressurized or liquefied hydrogen in gaseous tubes (100–350 bar) or liquid tank trailers (20 K) are the main delivery modes in the present stage.[144] Hydrogen liquification requires a higher energy consumption and a lower storage temperature than liquefied natural gas (LNG), significantly increasing the cost. Cryo-compressed hydrogen (200 K, 700 bar or higher) for delivery is attracting substantial attention because it has a much higher volumetric energy density than compressed gaseous hydrogen and a lower energy consumption level than liquid hydrogen.[147] In addition, a good match of the hydrogen state (pressure and temperature) between delivery and end use can obviously reduce the cost. The implementation of trailers for hydrogen delivery applications has a low capital cost and provides good investment flexibility. However, by enlarging the delivery scale, this technique loses its economic advantages because both the capital and operation costs grow linearly. To date, pipelines are widely recognized as the most economical mode for large-scale hydrogen delivery. Studies by the European Union (EU) show that the levelized cost of hydrogen delivery by pipeline is USD 0.11–0.20 kg^{-1} H$_2$ per 1000 km.[148] Although the estimated values of this cost vary considerably in different studies due to the lack of sufficient examples of hydrogen pipelines, it is still widely acknowledged that this cost only occupies a relatively small fraction of the total cost for delivery in a mature hydrogen society. Hydrogen pipelines can repurpose existing natural gas (NG) transmission networks with appropriate modifications, significantly reducing the initial investment, and the repurpose cost is approximately 10–33% of the cost of building new hydrogen pipelines.[149] Developing pipeline materials (with low cost, low sensitivity to hydrogen embrittlement, low leakage rate and good high-pressure resistance) and compressor technologies with high efficiency are the main technical challenges. Furthermore, the recent bottlenecks in developing hydrogen pipelines still mainly lie in the low hydrogen supply-and-demand capacity, high initial investment for the low hydrogen market, safety issues, and social acceptance. Blending hydrogen in NG pipeline networks as a fuel component, mainly for combustion applications, is an important approach to hydrogen delivery and use to reduce the use of fossil energy.[150] The issues of pipeline modification costs, safety, and end-use modifications should be considered based on different blending proportions of 5–50% hydrogen in gas. However, it is still not cost-effective to purify hydrogen from the blending gas.

Converting hydrogen into liquid hydrogen carriers to readily store and transport it for delivery is an important route (Fig. 5a).[151] Ammonia and methanol are widely recognized carriers, and some other liquid organic hydrogen carriers (LOHCs), such as benzene and naphthalene, are still being researched. Increasing the hydrogen storage capacity and decreasing the (de)hydrogenation temperature of carriers are the targets for material selection and development.[136,152] The delivery process generally consists of centralized hydrogen carrier synthesis (conditioning), hydrogen carrier delivery,

dehydrogenation and purification (reconditioning), and possible byproduct recovery. The storage and delivery of hydrogen carriers can exert full advantages of the existing infrastructures; thus, its capital cost is lower than that of building a new hydrogen pipeline, and its delivery cost can be generally lower than that of liquid hydrogen. However, the synthesis and dehydrogenation processes require substantial energy consumption and economic cost levels. For example, ammonia synthesis and cracking consume approximately 7–18% of the energy of the corresponding hydrogen;[148] the ideal state is that this energy consumption can come from the waste heat of industrial sources. Therefore, the delivery of hydrogen carriers is generally suitable for ultralarge-scale delivery or scenarios not suitable for pipeline construction in a future hydrogen society. Developing efficient and low-cost catalysts and reactors for hydrogen carrier synthesis and dehydrogenation are key technical issues for improving the maturity and reducing the cost of the hydrogen carrier delivery route. The miniaturized onboard dehydrogenation reactor for automotive applications using a hydrogen carrier as a fuel is viewed as a potential solution. In addition, with technical maturity improvement and cost reduction, material-based hydrogen storage methods have the prospects to be applied in hydrogen delivery in the future. Overall, a preliminary selection of the economic hydrogen delivery route can be generally achieved regarding the delivery volume and distance; the EU has provided the following strict yet directional suggestions.[153] Trailers are suitable for small-scale hydrogen delivery (volume of approximately less than 10 tons H$_2$ per day and distance of less than 200 km). The pipeline is the best choice for large-scale delivery (more than approximately 10 tons H$_2$ per day) in long-range transmission and short-range distribution. Hydrogen carrier shipment is considered especially for ultralarge-scale and intercontinental delivery (more than approximately 100 tons H$_2$ per day).

Hydrogen refuelling stations are both the terminals of hydrogen-delivery networks and the hydrogen sources for FCVs. The regional distribution densities of refuelling stations should match the market penetration of FCVs, where the lack of access is an important factor limiting the large-scale commercialization of FCVs in the present stage. The cost of refuelling stations still occupies a large proportion of that of hydrogen end-use sales to date. With increasing market penetration of FCVs, especially commercial vehicles, the size of refuelling stations is significantly enlarged, and the levelized capital costs of refuelling stations (USD kg^{-1} H$_2$ per day) decrease following the scale effect.[154] Based on the location of hydrogen production, refuelling stations can be divided into off-site and on-site stations. For the off-site station, hydrogen is transported from the centralized hydrogen production facilities, and the station only serves short-term hydrogen storage and hydrogen dispensing to FCVs. The primary and costly equipment in stations includes compressors, hydrogen storage tanks, dispensers, and precoolers. For future development, reducing the capital cost and improving the efficiency of a stationary small-scale compressor, reducing the capital cost of a hydrogen storage tank, increasing the hydrogen circulating efficiency by appropriate

demand forecasting and planning, and designing fast and safe refuelling strategies should be considered at the station level. In addition, the on-site station produces and dispenses hydrogen inside the station *via* stationary water electrolysis devices or hydrogen carrier reformers.[155] Relative to centralized hydrogen production, the cost of stationary hydrogen production is higher due to the utilization of expensive small-scale devices, compressors, and renewable electricity. Therefore, a clear trade-off between the costs of hydrogen production and delivery generally exists.[144] In general, the two routes (off-site and on-site stations) are promising, and the issues of cost and safety are the main measurable factors for choosing a comprehensive route.

From this perspective, we give two hypothetical scenarios, design detailed routes of hydrogen production and delivery, and calculate their total levelized cost of hydrogen (LCOH) at the refuelling station. Notably, the renewable electricity prize highly influences the costs of hydrogen production and delivery, and it keeps decreasing with the rapid development of renewable generation facilities, such as photovoltaic (PV) and onshore/offshore wind facilities. Thus, a reduced renewable electricity prize in the future is assumed and used in our calculations. The first scenario is hydrogen delivery within the continent, from renewable-rich regions to energy-consuming regions, where we take the example of hydrogen transport from Gansu Province to Shanghai, China (approximately 2000 km, see Fig. 5b for results and Supplementary Note 1 and Tables S2 and S7–S10, ESI† for specific parameters). In this case, the transmission is conducted by transporting through a hydrogen pipeline or by repurposing an NG pipeline; distribution is conducted by city pipeline networks or compressed gas tube trailers. Notably, the difference in hydrogen pressure between the two distribution methods leads to a difference in the cost of refuelling. In addition, the route of stationary hydrogen production is considered. The calculations show that through the route of centralized hydrogen production, by repurposing the NG pipeline for transmission and the tube trailers for distribution and determining the corresponding refuelling (*i.e.*, 1-b-II route in Fig. 5b), the terminal cost of hydrogen at the refuelling station can be less than USD 4 kg^{-1} H$_2$; additionally, the delivery cost (<USD 2 kg^{-1} H$_2$) is less than half of the total cost, which can meet the economic goal proposed by the DOE. The adoption of a hydrogen pipeline for transmission increases the cost to over USD 4 kg^{-1} H$_2$ due to the high initial capital cost; the corresponding cost should be reduced with the further increase in delivery scale and service life. Moreover, the cost of the route of stationary hydrogen production highly depends on the local electricity price. The second scenario is intercontinental hydrogen delivery, for which we use hydrogen transport from Australia to Japan as an example (approximately 7500 km; for results, see Fig. 5c; for specific parameters, see Supplementary Note 1 and Tables S2, S8–S17, ESI†). The transmission is conducted by the shipment of liquid hydrogen and hydrogen carriers (ammonia and methanol). Although reconditioning from carriers to hydrogen leads to the substantial cost, the total costs of carrier delivery are still lower than those of liquid hydrogen delivery in this hypothetical scenario; furthermore, the terminal

cost of hydrogen after adopting either ammonia or methanol as a carrier in the delivery route is approximately USD 7 kg^{-1} H$_2$.

6. Hydrogen use

Hydrogen is broadly applicable in the fuel, biorefining, metallurgy, aerospace, and pharmaceutical industries. Herein, we emphasize hydrogen as an energy vector. Fuel cells are widely recognized as optimal power devices for hydrogen use to date. Two types of cells, PEMFCs with operating temperatures below 100 °C and SOFCs with operating temperatures of 350–1200 °C, have attracted substantial attention due to their relatively high technical maturity and commercialization among various kinds of fuel cells.[156–158]

PEMFC shows the advantages of high conversion efficiency (40–60%), fast dynamic response, and good modularity and is the closest to the mass market relative to other types of fuel cells.[159] The PEMFC stack is considered a promising choice for stationary and portable applications, especially in the field of FCVs. However, breakthroughs in the system cost and durability of PEMFC stacks (<USD 76 kW^{-1} and >8000 h) are still needed to propel the commercialization process.[160] Continuous development of high-performance material systems with acceptable prices and properly optimized cell structure designs are critical for increasing the stack power density. For basic material development, novel Pt-based catalyst systems with modified compositions and structures are highly capable of boosting the specific activity and stability, such as Pt alloys,[161–164] strained Pt electrodes,[165] microstrained Pt-based catalysts,[166] Pt nanostructures,[167,168] and Pt concave nanoparticles and cavities.[169,170] In addition, carbon-based materials doped with nitrogen and transition metals have made impressive achievements in replacing Pt-based catalysts for fuel cells.[171–174] In the next 5–10 years, Pt alloys with micromodifications or nanomodifications can still be the mainstream catalysts for fuel cells due to their comprehensive advantages in terms of performance, durability, maturity, and cost. For cell design, order-structured membrane electrode assembly (MEA) and integrated bipolar plate-MEA (BP-MEA) designs are promising directions for next-generation PEMFCs due to their potential in building highly efficient mass transport pathways and achieving high power density at ultralow catalyst loading.[157] Moreover, with the increase in market scale, the situation can be improved, especially from the cost perspective; this shows potential for developing an extensive and comprehensive infrastructure distribution.

With high efficiency and broad application prospects, SOFCs have good fuel adaptability and flexibility and can directly use crude hydrogen, ammonia, and various hydrocarbon fuels, such as biomass gas. SOFCs are very promising in thermal-electric cogeneration applications relative to other cells, and the overall efficiency can exceed 90% when heat is effectively utilized.[157] In this stage, the development of SOFCs is focused on reducing the cost and improving the durability (DOE targets of <USD 450 kW^{-1} and >40 000 h).[157] The following aspects should be achieved to enable the low-cost and stable production of industrial-sized single cell batches: (i) optimizing the

This journal is © The Royal Society of Chemistry 2023

Energy Environ. Sci., 2023, **16**, 4926–4943 | **4937**

low-temperature preparation methods of dense thin-film electrolytes; (ii) improving the electrochemical activity of the cathode and inhibiting delamination and chemical diffusion at the electrode–electrolyte interface; (iii) strengthening the resistance of the anode to coarsening, carbon deposition and redox cycling; (iv) developing new and promising composite sealing materials; and (v) exploring cell durability with accelerated experimental methods. In the long run, achieving low-temperature (350–600 °C) operation will continue to be the mainstream development trend of SOFCs.[158] The development of cathodes with high electrochemical catalytic activities at low temperatures and the use of proton-conducting electrolytes are the main methods for reducing the operating temperature, requiring long-term research. Proton ceramic fuel cells (PCFCs) conduct much smaller protons and have lower activation energies than oxygen ion-conducting SOFCs, thus offering attractive potential for high-performance and low-temperature operation.[175] In addition, SOFC can operate reversely as an electrolyser (a reversible solid oxide cell (RSOC)), which can effectively reduce the complexity and improve the flexibility between hydrogen-to-electricity and electricity-to-hydrogen modes in the future hydrogen society.

7. Summary and outlook

Although the current proportion of hydrogen energy in the total final energy-consumption system is small, hydrogen will remain in high demand when realizing a sustainable society due to its important and indispensable roles in production, living, the environment, and the economy. This demand is pushing the development of related technologies for hydrogen production, storage, delivery, and usage.

Regarding hydrogen production, renewable and sustainable green hydrogen production is expected to replace the traditional grey hydrogen and blue hydrogen production modes in the future due to the presence of the lowest future cost of ~ 1 USD kg^{-1} H_2. However, high cost is a major barrier for the development of green hydrogen production. Systematic analysis of the advantages and disadvantages of representative technologies, such as AWE, AEME, PEME, SOEC and PCEC, is conducted to note their development directions. Our techno-economic calculations reveal that the major cost of the above technologies originates from their high consumption of electricity, where the different electricity prices in different regions lead to very high hydrogen supply-and-demand gaps, and they facilitate global hydrogen flows. This phenomenon calls for the advancement of power-generation technologies. Moreover, developing and screening efficient and robust electrocatalyst candidates is key for reducing electricity consumption and production costs. From catalyst morphologies, macroscopic physiochemical properties, molecular-level structural information and electronic structural features, we offer comprehensive and robust insights into the rational design of promising electrocatalysts. Furthermore, an effective framework for screening potential material candidates based on big data

and artificial intelligence is given, aimed at constantly updating the optimal electrode electrocatalysts to reduce the cost and accelerate the commercialization of green hydrogen production.

Storing hydrogen in a dense and safe manner remains a critical challenge. Commercially, physical-based hydrogen storage exhibits high acceptance and limited energy density. The scientific community places great importance on material-based hydrogen storage for on-board applications, where most solid-state chemisorption systems need to overcome the kinetic and thermodynamic obstacles to reduce the dehydrogenation temperature below the target of 85 °C proposed by DOE with a guaranteed hydrogen storage capacity (>6.5 wt%). Experimental strategies, such as nanostructuring, catalysis, compositing and surface/interface engineering, have offered promising solutions to these intrinsic limitations. New kinds of hydrogen-storage material development and performance prediction based on machine learning and big data should be expected, although very few works have been undertaken in the recent field. The design and management of hydrogen, thermal, and electric coupling should be carefully considered in a practical hydrogen storage-consumption system.

Reducing the cost of hydrogen delivery to meet the DOE target of the terminal cost at the refuelling station with less than USD 4 kg^{-1} H_2 and a delivery cost of less than USD 2 kg^{-1} H_2 is a cornerstone for a mature hydrogen society. The delivery process generally consists of transmission, distribution and dispensing with different transport scales. The shipment of hydrogen carriers, large-scale transport by hydrogen pipelines, small-scale transport by trailers, repurposing of NG pipelines, blending of hydrogen into NG, and distributed/stationary hydrogen production are all potential and promising modes. These modes can be properly combined to constitute a multi-level delivery route based on specific scenarios, including the factors of volume, distance, geographic conditions, circulating period, policies, and safety. Our original techno-economic calculations show that with a reasonable route design for hydrogen production and delivery, the terminal cost at the refuelling station can meet the DOE cost target.

For hydrogen use, fuel cells are indispensable for hydrogen applications, among which PEMFCs and SOFCs already show relatively high technological maturity. Developing the basic materials and design of the cells and systems is still urgently required to further improve the efficiency, prolong the durability, and reduce the cost for the large-scale commercialization of fuel cells in a hydrogen society.

Author contributions

M. Ni and K. Jiao proposed, conceived and funded this study. Z. Shao gave valuable comments and suggestions on the manuscript. D. Guan, B. Wang and J. Zhang were responsible to the contents of hydrogen production, delivery and storage, respectively. R. Shi and L. Li contributed to the writing of hydrogen storage and the calculations of technological economics, respectively. Y. Wang and B. Xie wrote the part of hydrogen

4938 | Energy Environ. Sci., 2023, 16, 4926–4943

This journal is © The Royal Society of Chemistry 2023

usage. Q. Zhang, J. Yu and Y. Zhu took part in the data collection of techno-economic calculations, hydrogen production and hydrogen storage, respectively. D. Guan, B. Wang, M. Ni, K. Jiao and Z. Shao integrated all the parts and revised the manuscript to the final version.

Conflicts of interest

There are no conflicts to declare.

Acknowledgements

References

1 G. M. Whitesides and G. W. Crabtree, *Science*, 2007, **315**, 796–798.

2 World energy transitions outlook: 1.5 °C pathway, International Renewable Energy Agency, 2021.

3 Hydrogen from renewable power: technology outlook for the energy transition, International Renewable Energy Agency, 2018.

4 Z. W. Seh, J. Kibsgaard, C. F. Dickens, I. Chorkendorff, J. K. Nørskov and T. F. Jaramillo, *Science*, 2017, **355**, eaad4998.

5 Net zero by 2050: a roadmap for the global energy sector, International Energy Agency, 2021.

6 Global hydrogen review 2021, International Energy Agency, 2021.

7 Green hydrogen cost reduction: scaling up electrolysers to meet the 1.5 °C climate goal, International Renewable Energy Agency, 2020.

8 Hydrogen for net-zero: a critical cost-competitive energy vector, Hydrogen Council and McKinsey & Company, 2021.

9 T. Braun and K. Baert, Coal vs methane vs water: the future of hydrogen production, Kawasaki Heavy Industries, 2022.

10 Hydrogen insights: a perspective on hydrogen investment, market development and cost competitiveness, Hydrogen Council and McKinsey & Company, 2021.

11 K. Zeng and D. Zhang, *Prog. Energy Combust. Sci.*, 2010, **36**, 307–326.

12 C. Duan, J. Huang, N. Sullivan and R. O'Hayre, *Appl. Phys. Rev.*, 2020, **7**, 011314.

13 A. Fujishima and K. Honda, *Nature*, 1972, **238**, 37–38.

14 H. Nishiyama, T. Yamada, M. Nakabayashi, Y. Maehara, M. Yamaguchi, Y. Kuromiya, Y. Nagatsuma, H. Tokudome, S. Akiyama, T. Watanabe, R. Narushima, S. Okunaka, N. Shibata, T. Takata, T. Hisatomi and K. Domen, *Nature*, 2021, **598**, 304–307.

15 P. Zhou, I. A. Navid, Y. Ma, Y. Xiao, P. Wang, Z. Ye, B. Zhou, K. Sun and Z. Mi, *Nature*, 2023, **613**, 66–70.

16 T. Hisatomi and K. Domen, *Nat. Catal.*, 2019, **2**, 387–399.

17 X. Li, X. Sun, Q. Song, Z. Yang, H. Wang and Y. Duan, *Int. J. Hydrogen Energy*, 2022, **47**, 33619–33642.

18 W. C. Chueh, C. Falter, M. Abbott, D. Scipio, P. Furler, S. M. Haile and A. Steinfeld, *Science*, 2010, **330**, 1797–1801.

19 R. Schäppi, D. Rutz, F. Dähler, A. Muroyama, P. Haueter, J. Lilliestam, A. Patt, P. Furler and A. Steinfeld, *Nature*, 2022, **601**, 63–68.

20 J. Jia, L. C. Seitz, J. D. Benck, Y. Huo, Y. Chen, J. W. Ng, T. Bilir, J. S. Harris and T. F. Jaramillo, *Nat. Commun.*, 2016, **7**, 13237.

21 Electricity market report, International Energy Agency, 2022.

22 Global hydrogen flows: hydrogen trade as a key enabler for efficient decarbonization, Hydrogen Council and McKinsey & Company, 2022.

23 Y. Jiao, Y. Zheng, M. Jaroniec and S. Z. Qiao, *Chem. Soc. Rev.*, 2015, **44**, 2060–2086.

24 Z. Zhou, Z. Pei, L. Wei, S. Zhao, X. Jian and Y. Chen, *Energy Environ. Sci.*, 2020, **13**, 3185–3206.

25 W. Tong, M. Forster, F. Dionigi, S. Dresp, R. Sadeghi Erami, P. Strasser, A. J. Cowan and P. Farràs, *Nat. Energy*, 2020, **5**, 367–377.

26 W. Zhang, M. Liu, X. Gu, Y. Shi, Z. Deng and N. Cai, *Chem. Rev.*, 2023, **123**, 7119–7192.

27 P. C. K. Vesborg and T. F. Jaramillo, *RSC Adv.*, 2012, **2**, 7933–7947.

28 J. Greeley, T. F. Jaramillo, J. Bonde, I. Chorkendorff and J. K. Nørskov, *Nat. Mater.*, 2006, **5**, 909–913.

29 T. F. Jaramillo, K. P. Jørgensen, J. Bonde, J. H. Nielsen, S. Horch and I. Chorkendorff, *Science*, 2007, **317**, 100–102.

30 J. D. Benck, T. R. Hellstern, J. Kibsgaard, P. Chakthranont and T. F. Jaramillo, *ACS Catal.*, 2014, **4**, 3957–3971.

31 W. F. Chen, K. Sasaki, C. Ma, A. I. Frenkel, N. Marinkovic, J. T. Muckerman, Y. Zhu and R. R. Adzic, *Angew. Chem., Int. Ed.*, 2012, **51**, 6131–6135.

32 D. Kong, J. J. Cha, H. Wang, H. R. Lee and Y. Cui, *Energy Environ. Sci.*, 2013, **6**, 3553–3558.

33 E. J. Popczun, J. R. McKone, C. G. Read, A. J. Biacchi, A. M. Wiltrout, N. S. Lewis and R. E. Schaak, *J. Am. Chem. Soc.*, 2013, **135**, 9267–9270.

34 W. F. Chen, C. H. Wang, K. Sasaki, N. Marinkovic, W. Xu, J. T. Muckerman, Y. Zhu and R. R. Adzic, *Energy Environ. Sci.*, 2013, **6**, 943–951.

35 Z. W. Seh, K. D. Fredrickson, B. Anasori, J. Kibsgaard, A. L. Strickler, M. R. Lukatskaya, Y. Gogotsi, T. F. Jaramillo and A. Vojvodic, *ACS Energy Lett.*, 2016, **1**, 589–594.

36 Y. Zheng, Y. Jiao, Y. Zhu, L. H. Li, Y. Han, Y. Chen, A. Du, M. Jaroniec and S. Z. Qiao, *Nat. Commun.*, 2014, **5**, 3783.

37 S. Geiger, O. Kasian, M. Ledendecker, E. Pizzutilo, A. M. Mingers, W. T. Fu, O. Diaz-Morales, Z. Li, T. Oellers, L. Fruchter, A. Ludwig, K. J. J. Mayrhofer, M. T. M. Koper and S. Cherevko, *Nat. Catal.*, 2018, **1**, 508–515.

This journal is © The Royal Society of Chemistry 2023

Energy Environ. Sci., 2023, **16**, 4926–4943 | **4939**

38 L. An, C. Wei, M. Lu, H. Liu, Y. Chen, G. G. Scherer, A. C. Fisher, P. Xi, Z. J. Xu and C. H. Yan, *Adv. Mater.*, 2021, **33**, 2006328.

39 L. Chong, G. Gao, J. Wen, H. Li, H. Xu, Z. Green, J. D. Sugar, A. J. Kropf, W. Xu, X. Lin, H. Xu, L. Wang and D. J. Liu, *Science*, 2023, **380**, 609–616.

40 A. Li, S. Kong, C. Guo, H. Ooka, K. Adachi, D. Hashizume, Q. Jiang, H. Han, J. Xiao and R. Nakamura, *Nat. Catal.*, 2022, **5**, 109–118.

41 A. Li, H. Ooka, N. Bonnet, T. Hayashi, Y. Sun, Q. Jiang, C. Li, H. Han and R. Nakamura, *Angew. Chem., Int. Ed.*, 2019, **58**, 5054–5058.

42 M. Blasco-Ahicart, J. Soriano-Lopez, J. J. Carbo, J. M. Poblet and J. R. Galan-Mascaros, *Nat. Chem.*, 2018, **10**, 24–30.

43 W. Yin, B. Weng, J. Ge, Q. Sun, Z. Li and Y. Yan, *Energy Environ. Sci.*, 2019, **12**, 442–462.

44 Q. Zhao, Z. Yan, C. Chen and J. Chen, *Chem. Rev.*, 2017, **117**, 10121–10211.

45 D. Zhou, P. Li, X. Lin, A. McKinley, Y. Kuang, W. Liu, W. F. Lin, X. Sun and X. Duan, *Chem. Soc. Rev.*, 2021, **50**, 8790–8817.

46 I. Ledezma-Yanez, W. D. Z. Wallace, P. Sebastián-Pascual, V. Climent, J. M. Feliu and M. T. M. Koper, *Nat. Energy*, 2017, **2**, 1–7.

47 W. Sheng, H. A. Gasteiger and Y. Shao-Horn, *J. Electrochem. Soc.*, 2010, **157**, B1529–B1536.

48 M. A. Hubert, A. M. Patel, A. Gallo, Y. Liu, E. Valle, M. Ben-Naim, J. Sanchez, D. Sokaras, R. Sinclair, J. K. Nørskov, L. A. King, M. Bajdich and T. F. Jaramillo, *ACS Catal.*, 2020, **10**, 12182–12196.

49 D. Galyamin, J. Torrero, I. Rodriguez, M. J. Kolb, P. Ferrer, L. Pascual, M. A. Salam, D. Gianolio, V. Celorrio, M. Mokhtar, D. Garcia Sanchez, A. S. Gago, K. A. Friedrich, M. A. Pena, J. A. Alonso, F. Calle-Vallejo, M. Retuerto and S. Rojas, *Nat. Commun.*, 2023, **14**, 2010.

50 D. Strmcnik, M. Uchimura, C. Wang, R. Subbaraman, N. Danilovic, D. van der Vliet, A. P. Paulikas, V. R. Stamenkovic and N. M. Markovic, *Nat. Chem.*, 2013, **5**, 300–306.

51 W. T. Hong, M. Risch, K. A. Stoerzinger, A. Grimaud, J. Suntivich and Y. Shao-Horn, *Energy Environ. Sci.*, 2015, **8**, 1404–1427.

52 Y. Xu, C. Wang, Y. Huang and J. Fu, *Nano Energy*, 2021, **80**, 105545.

53 C.-T. Dinh, A. Jain, F. P. G. de Arquer, P. De Luna, J. Li, N. Wang, X. Zheng, J. Cai, B. Z. Gregory, O. Voznyy, B. Zhang, M. Liu, D. Sinton, E. J. Crumlin and E. H. Sargent, *Nat. Energy*, 2018, **4**, 107–114.

54 J. N. Hausmann, R. Schlögl, P. W. Menezes and M. Driess, *Energy Environ. Sci.*, 2021, **14**, 3679–3685.

55 H. Xie, Z. Zhao, T. Liu, Y. Wu, C. Lan, W. Jiang, L. Zhu, Y. Wang, D. Yang and Z. Shao, *Nature*, 2022, **612**, 673–678.

56 J. Guo, Y. Zhang, A. Zavabeti, K. Chen, Y. Guo, G. Hu, X. Fan and G. K. Li, *Nat. Commun.*, 2022, **13**, 5046.

57 Y. Wang, H. Su, Y. He, L. Li, S. Zhu, H. Shen, P. Xie, X. Fu, G. Zhou, C. Feng, D. Zhao, F. Xiao, X. Zhu, Y. Zeng,

58 D. A. Corrigan, *J. Electrochem. Soc.*, 1987, **134**, 377–384.

59 M. S. Burke, M. G. Kast, L. Trotochaud, A. M. Smith and S. W. Boettcher, *J. Am. Chem. Soc.*, 2015, **137**, 3638–3648.

60 Y. Zhang, T. T. Zuo, Z. Tang, M. C. Gao, K. A. Dahmen, P. K. Liaw and Z. P. Lu, *Prog. Mater. Sci.*, 2014, **61**, 1–93.

61 X. Xu, Z. Shao and S. P. Jiang, *Energy Technol.*, 2022, **10**, 2200573.

62 G. Liu, W. S. Y. Wong, M. Kraft, J. W. Ager, D. Vollmer and R. Xu, *Chem. Soc. Rev.*, 2021, **50**, 10674–10699.

63 T. Young, *Philos. Trans. R. Soc. London*, 1805, **95**, 65–87.

64 T. Wu, X. Ren, Y. Sun, S. Sun, G. Xian, G. G. Scherer, A. C. Fisher, D. Mandler, J. W. Ager, A. Grimaud, J. Wang, C. Shen, H. Yang, J. Gracia, H. J. Gao and Z. J. Xu, *Nat. Commun.*, 2021, **12**, 3634.

65 J. Ge, R. R. Chen, X. Ren, J. Liu, S. J. H. Ong and Z. J. Xu, *Adv. Mater.*, 2021, **33**, 2101091.

66 P. G. De Gennes, *Phys. Rev.*, 1960, **118**, 141–154.

67 Y. Tong, J. Wu, P. Chen, H. Liu, W. Chu, C. Wu and Y. Xie, *J. Am. Chem. Soc.*, 2018, **140**, 11165–11169.

68 D. Guan, J. Zhou, Z. Hu, W. Zhou, X. Xu, Y. Zhong, B. Liu, Y. Chen, M. Xu, H. J. Lin, C. T. Chen, J. Wang and Z. Shao, *Adv. Funct. Mater.*, 2019, **29**, 1900704.

69 A. Grimaud, C. E. Carlton, M. Risch, W. T. Hong, K. J. May and Y. Shao-Horn, *J. Phys. Chem. C*, 2013, **117**, 25926–25932.

70 Y. Chen, J. K. Seo, Y. Sun, T. A. Wynn, M. Olguin, M. Zhang, J. Wang, S. Xi, Y. Du, K. Yuan, W. Chen, A. C. Fisher, M. Wang, Z. Feng, J. Gracia, L. Huang, S. Du, H. J. Gao, Y. S. Meng and Z. J. Xu, *Nat. Commun.*, 2022, **13**, 5510.

71 M. Risch, A. Grimaud, K. J. May, K. A. Stoerzinger, T. J. Chen, A. N. Mansour and Y. Shao-Horn, *J. Phys. Chem. C*, 2013, **117**, 8628–8635.

72 D. Guan, K. Zhang, Z. Hu, X. Wu, J. L. Chen, C. W. Pao, Y. Guo, W. Zhou and Z. Shao, *Adv. Mater.*, 2021, **33**, 2103392.

73 C. W. Song, J. Lim, H. B. Bae and S.-Y. Chung, *Energy Environ. Sci.*, 2020, **13**, 4178–4188.

74 D. Guan, G. Ryu, Z. Hu, J. Zhou, C.-L. Dong, Y.-C. Huang, K. Zhang, Y. Zhong, A. C. Komarek, M. Zhu, X. Wu, C.-W. Pao, C.-K. Chang, H.-J. Lin, C.-T. Chen, W. Zhou and Z. Shao, *Nat. Commun.*, 2020, **11**, 3376.

75 J. Hwang, Z. Feng, N. Charles, X. R. Wang, D. Lee, K. A. Stoerzinger, S. Muy, R. R. Rao, D. Lee, R. Jacobs, D. Morgan and Y. Shao-Horn, *Mater. Today*, 2019, **31**, 100–118.

76 H. Ding, H. Liu, W. Chu, C. Wu and Y. Xie, *Chem. Rev.*, 2021, **121**, 13174–13212.

77 F. De Groot, Z. Hu, M. Lopez, G. Kaindl, F. Guillou and M. Tronc, *J. Chem. Phys.*, 1994, **101**, 6570–6576.

78 J. Hwang, R. R. Rao, L. Giordano, Y. Katayama, Y. Yu and Y. Shao-Horn, *Science*, 2017, **358**, 751–756.

79 V. Bisogni, S. Catalano, R. J. Green, M. Gibert, R. Scherwitzl, Y. Huang, V. N. Strocov, P. Zubko, S. Balandeh, J. M. Triscone, G. Sawatzky and T. Schmitt, *Nat. Commun.*, 2016, **7**, 13017.

4940 | *Energy Environ. Sci.*, 2023, **16**, 4926–4943

This journal is © The Royal Society of Chemistry 2023

80 J. Suntivich, K. J. May, H. A. Gasteiger, J. B. Goodenough and Y. Shao-Horn, *Science*, 2011, **334**, 1383–1385.

81 Y. Sun, H. Liao, J. Wang, B. Chen, S. Sun, S. J. H. Ong, S. Xi, C. Diao, Y. Du, J.-O. Wang, M. B. H. Breese, S. Li, H. Zhang and Z. J. Xu, *Nat. Catal.*, 2020, **3**, 554–563.

82 A. Grimaud, K. J. May, C. E. Carlton, Y. L. Lee, M. Risch, W. T. Hong, J. Zhou and Y. Shao-Horn, *Nat. Commun.*, 2013, **4**, 2439.

83 W. T. Hong, K. A. Stoerzinger, Y.-L. Lee, L. Giordano, A. Grimaud, A. M. Johnson, J. Hwang, E. J. Crumlin, W. Yang and Y. Shao-Horn, *Energy Environ. Sci.*, 2017, **10**, 2190–2200.

84 D. Cao, H. Xu, H. Li, C. Feng, J. Zeng and D. Cheng, *Nat. Commun.*, 2022, **13**, 5843.

85 G. Van der Laan, J. Zaanen, G. A. Sawatzky, R. Karnatak and J. M. Esteva, *Phys. Rev. B: Condens. Matter Mater. Phys.*, 1986, **33**, 4253–4263.

86 D. Guan, K. Zhang, W. Zhou and Z. Shao, *Curr. Opin. Electrochem.*, 2021, **30**, 100805.

87 A. E. Bocquet, T. Mizokawa, T. Saitoh, H. Namatame and A. Fujimori, *Phys. Rev. B: Condens. Matter Mater. Phys.*, 1992, **46**, 3771–3784.

88 R. H. Potze, G. A. Sawatzky and M. Abbate, *Phys. Rev. B: Condens. Matter Mater. Phys.*, 1995, **51**, 11501–11506.

89 A. Grimaud, O. Diaz-Morales, B. Han, W. T. Hong, Y. L. Lee, L. Giordano, K. A. Stoerzinger, M. T. M. Koper and Y. Shao-Horn, *Nat. Chem.*, 2017, **9**, 457–465.

90 B. Weng, Z. Song, R. Zhu, Q. Yan, Q. Sun, C. G. Grice, Y. Yan and W. J. Yin, *Nat. Commun.*, 2020, **11**, 3513.

91 L. Han, H. Cheng, W. Liu, H. Li, P. Ou, R. Lin, H. T. Wang, C. W. Pao, A. R. Head, C. H. Wang, X. Tong, C. J. Sun, W. F. Pong, J. Luo, J. C. Zheng and H. L. Xin, *Nat. Mater.*, 2022, **21**, 681–688.

92 J. Rossmeisl, Z. W. Qu, H. Zhu, G. J. Kroes and J. K. Nørskov, *J. Electroanal. Chem.*, 2007, **607**, 83–89.

93 I. C. Man, H.-Y. Su, F. Calle-Vallejo, H. A. Hansen, J. I. Martínez, N. G. Inoglu, J. Kitchin, T. F. Jaramillo, J. K. Nørskov and J. Rossmeisl, *ChemCatChem*, 2011, **3**, 1159–1165.

94 O. Diaz-Morales, I. Ledezma-Yanez, M. T. M. Koper and F. Calle-Vallejo, *ACS Catal.*, 2015, **5**, 5380–5387.

95 B. Hammer and J. K. Nørskov, *Nature*, 1995, **376**, 238–240.

96 Y.-L. Lee, J. Kleis, J. Rossmeisl, Y. Shao-Horn and D. Morgan, *Energy Environ. Sci.*, 2011, **4**, 3966–3970.

97 R. Jacobs, J. Hwang, Y. Shao-Horn and D. Morgan, *Chem. Mater.*, 2019, **31**, 785–797.

98 D. Guan, H. Xu, Q. Zhang, Y. C. Huang, C. Shi, Y. C. Chang, X. Xu, J. Tang, Y. Gu, C. W. Pao, S. C. Haw, J. M. Chen, Z. Hu, M. Ni and Z. Shao, *Adv. Mater.*, 2023, 2305704, DOI: **10.1002/adma.202305074.**

99 F. Calle-Vallejo, N. G. Inoglu, H.-Y. Su, J. I. Martínez, I. C. Man, M. T. M. Koper, J. R. Kitchin and J. Rossmeisl, *Chem. Sci.*, 2013, **4**, 1245.

100 D. Guan, J. Zhou, Y. C. Huang, C. L. Dong, J. Q. Wang, W. Zhou and Z. Shao, *Nat. Commun.*, 2019, **10**, 3755.

101 J. O. M. Bockris and T. Otagawa, *J. Electrochem. Soc.*, 1984, **131**, 290–302.

102 D. Wu, C. Dong, H. Zhan and X. W. Du, *J. Phys. Chem. Lett.*, 2018, **9**, 3387–3391.

103 T. He, W. Wang, F. Shi, X. Yang, X. Li, J. Wu, Y. Yin and M. Jin, *Nature*, 2021, **598**, 76–81.

104 Y. Dou, Y. Xie, X. Hao, T. Xia, Q. Li, J. Wang, L. Huo and H. Zhao, *Appl. Catal., B*, 2021, **297**, 120403.

105 X. Li, Y. Bai and Z. Cheng, *Adv. Sci.*, 2021, **8**, 2101000.

106 S. Trasatti, *J. Electroanal. Chem.*, 1980, **111**, 125–131.

107 F. Calle-Vallejo, O. A. Díaz-Morales, M. J. Kolb and M. T. M. Koper, *ACS Catal.*, 2015, **5**, 869–873.

108 O. Piqué, F. Illas and F. Calle-Vallejo, *Phys. Chem. Chem. Phys.*, 2020, **22**, 6797–6803.

109 K. S. Exner, *MethodsX*, 2021, **8**, 101590.

110 X. Cheng, E. Fabbri, Y. Yamashita, I. E. Castelli, B. Kim, M. Uchida, R. Haumont, I. Puente-Orench and T. J. Schmidt, *ACS Catal.*, 2018, **8**, 9567–9578.

111 S. Back, K. Tran and Z. W. Ulissi, *ACS Catal.*, 2019, **9**, 7651–7659.

112 J. Liu, W. Luo, L. Wang, J. Zhang, X. Z. Fu and J. L. Luo, *Adv. Funct. Mater.*, 2022, **32**, 2110748.

113 Z. Lin, S. Ou, A. Elgowainy, K. Reddi, M. Veenstra and L. Verduzco, *Appl. Energy*, 2018, **216**, 183–194.

114 H. Barthelemy, M. Weber and F. Barbier, *Int. J. Hydrogen Energy*, 2017, **42**, 7254–7262.

115 Y. Su, H. Lv, W. Zhou and C. Zhang, *World Electr. Veh. J.*, 2021, **12**, 130.

116 Onboard type IV compressed hydrogen storage system cost analysis, Department of Energy, 2016.

117 W. Balasooriya, C. Clute, B. Schrittesser and G. Pinter, *Polym. Rev.*, 2021, **62**, 175–209.

118 M. Aziz, *Energies*, 2021, **14**, 5917.

119 T. Brunner, M. Kampitsch and O. Kircher, *Fuel cells: data, facts, and figures-Chapter 17: cryo-compressed hydrogen storage*, Willey, 2016.

120 H. W. Langmi, N. Engelbrecht, P. M. Modisha and D. Bessarabov, *Electrochemical power sources: fundamentals, system, and applications-Chapter 13: hydrogen storage*, Elsevier, 2022.

121 Y. Kojima, H. Miyaoka and T. Ichikawa, *New and future developments in catalysis-Chapter 5: hydrogen storage materials*, Elsevier, 2013.

122 T. He, P. Pachfule, H. Wu, Q. Xu and P. Chen, *Nat. Rev. Mater.*, 2016, **1**, 16059.

123 R. C. Lochan, R. Z. Khaliullin and M. Head-Gordon, *Inorg. Chem.*, 2008, **47**, 4032–4044.

124 H. Kabbour, T. F. Baumann, J. H. Satcher, A. Saulnier and C. C. Ahn, *Chem. Mater.*, 2006, **18**, 6085–6087.

125 A. Ahmed and D. Siegel, *Patterns*, 2021, **2**, 100291.

126 X. Lu, Z. Xie, X. Wu, M. Li and W. Cai, *Chem. Eng. Sci.*, 2022, **259**, 117813.

127 J. Zhang, Y. Zhu, H. Lin, Y. Liu, Y. Zhang, S. Li, Z. Ma and L. Li, *Adv. Mater.*, 2017, **29**, 1700760.

128 K. J. Jeon, H. R. Moon, A. M. Ruminski, B. Jiang, C. Kisielowski, R. Bardhan and J. J. Urban, *Nat. Mater.*, 2011, **10**, 286–290.

129 E. S. Cho, A. M. Ruminski, S. Aloni, Y. S. Liu, J. Guo and J. J. Urban, *Nat. Commun.*, 2016, **7**, 10804.

130 A. Nakano, T. Maeda, H. Ito, T. Motyka, J. M. Perez-Berrios and S. Greenway, *Energy Procedia*, 2012, **29**, 463–468.

131 V. A. Yartys, M. Lototskyy, V. Linkov, D. Grant, A. Stuart, J. Eriksen, R. Denys and R. C. Bowman, *Appl. Phys. A: Mater. Sci. Process.*, 2016, **122**, 415.

132 A. Züttel, *Mater. Today*, 2003, **6**, 24–33.

133 T. Noritake, S. Towata, M. Aoki, Y. Seno, Y. Hirose, E. Nishibori, M. Takata and M. Sakata, *J. Alloys Compd.*, 2003, **356**, 84–86.

134 Z. Abdin and K. R. Khalipour, *Polygeneration with polystorage for chemical and energy hubs-Chapter 4: single and polystorage technologies for renewable-based hybrid energy systems*, Elsevier, 2019.

135 M. V. Solovev, O. V. Chashchikhin, P. V. Dorovatovskii, V. N. Khrustalev, A. S. Zyubin, T. S. Zyubina, O. V. Kravchenko, A. A. Zaytsev and Y. A. Dobrovolsky, *J. Power Sources*, 2018, **377**, 93–102.

136 Z. Abdin, C. Tang, Y. Liu and K. Catchpole, *iScience*, 2021, **24**, 102966.

137 M. Chandra and Q. Xu, *J. Power Sources*, 2007, **168**, 135–142.

138 W. Luo, L. N. Zakharov and S. Y. Liu, *J. Am. Chem. Soc.*, 2011, **133**, 13006–13009.

139 DOE technical targets for onboard hydrogen storage for light-duty vehicles, https://www.energy.gov/eere/fuelcells/doe-technical-targets-onboard-hydrogen-storage-light-duty-vehicles.

140 P. Chen and M. Zhu, *Mater. Today*, 2008, **11**, 36–43.

141 C. Wu and H.-M. Cheng, *J. Mater. Chem.*, 2010, **20**, 5390–5400.

142 H.-J. Lin, J.-J. Tang, Q. Yu, H. Wang, L.-Z. Ouyang, Y.-J. Zhao, J.-W. Liu, W.-H. Wang and M. Zhu, *Nano Energy*, 2014, **9**, 80–87.

143 C. Lu, Y. Ma, F. Li, H. Zhu, X. Zeng, W. Ding, T. Deng, J. Wu and J. Zou, *J. Mater. Chem. A*, 2019, **7**, 14629–14637.

144 Multi-year research, development, and demonstration plan-3.2 hydrogen delivery, Department of Energy, 2015.

145 K. Reddi, A. Elgowainy, N. Rustagi and E. Gupta, *Int. J. Hydrogen Energy*, 2017, **42**, 21855–21865.

146 C. Marino, A. Nucara, M. Pietrafesa and A. Pudano, *Energy*, 2013, **57**, 95–105.

147 J. Moreno-Blanco, G. Camacho, F. Valladares and S. M. Aceves, *Int. J. Hydrogen Energy*, 2020, **45**, 27369–27380.

148 Transporting pure hydrogen by repurposing existing gas infrastructure: overview of existing studies and reflections on the conditions for repurposing, European Union Agency for the Cooperation of Energy Regulators, 2021.

149 The European hydrogen backbone furthering energy independence, https://guidehouse.com/insights/energy/2022/european-hydrogen-backbone-energy-independence?lang=en.

150 M. W. Melaina, O. Antonia and M. Penev, *Blending hydrogen into natural gas pipeline networks: a review of key issues*, Department of Energy, 2013.

151 R. Dickson, M. S. Akhtar, A. Abbas, E. D. Park and J. Liu, *Green Chem.*, 2022, **24**, 8484–8493.

152 G. Sievi, D. Geburtig, T. Skeledzic, A. Bösmann, P. Preuster, O. Brummel, F. Waidhas, M. A. Montero, P. Khanipour, I. Katsounaros, J. Libuda, K. J. J. Mayrhofer and P. Wasserscheid, *Energy Environ. Sci.*, 2019, **12**, 2305–2314.

153 Making the hydrogen economy possible: accelerating clean hydrogen in an electrified economy, https://www.energy-transitions.org/publications/making-clean-hydrogen-possible/.

154 D. L. Greene, J. M. Ogden and Z. Lin, *eTransportation*, 2020, **6**, 100086.

155 G. Parks, R. Boyd, J. Cornish and R. Remick, *Blending hydrogen into natural gas pipeline networks: a review of key issues*, Department of Energy, 2013.

156 K. Jiao, J. Xuan, Q. Du, Z. Bao, B. Xie, B. Wang, Y. Zhao, L. Fan, H. Wang, Z. Hou, S. Huo, N. P. Brandon, Y. Yin and M. D. Guiver, *Nature*, 2021, **595**, 361–369.

157 1–10 kW stationary combined heat and power systems status and technical potential, Department of Energy, 2010.

158 E. D. Wachsman and K. T. Lee, *Science*, 2011, **334**, 935–939.

159 T. Ogawa, M. Takeuchi and Y. Kajikawa, *Sustainability*, 2018, **10**, 458.

160 2021 annual merit review and peer evaluation report, Department of Energy, 2021.

161 L. Chong, J. Wen, J. Kubal, F. G. Sen, J. Zou, J. Greeley, M. Chan, H. Barkholtz, W. Ding and D. Liu, *Science*, 2018, **362**, 1276–1281.

162 J. Greeley, I. E. Stephens, A. S. Bondarenko, T. P. Johansson, H. A. Hansen, T. F. Jaramillo, J. Rossmeisl, I. Chorkendorff and J. K. Norskøv, *Nat. Chem.*, 2009, **1**, 552–556.

163 V. Čolić and A. S. Bandarenka, *ACS Catal.*, 2016, **6**, 5378–5385.

164 R. M. Kluge, R. W. Haid, A. Riss, Y. Bao, K. Seufert, T. O. Schmidt, S. A. Watzele, J. V. Barth, F. Allegretti, W. Auwärter, F. Calle-Vallejo and A. S. Bandarenka, *Energy Environ. Sci.*, 2022, **15**, 5181–5191.

165 M. Escudero-Escribano, P. Malacrida, M. H. Hansen, U. G. Vej-Hansen, A. Velázquez-Palenzuela, V. Tripkovic, J. Schiøtz, J. Rossmeisl, I. E. Stephens and I. Chorkendorff, *Science*, 2016, **352**, 73–76.

166 R. Chattot, O. Le Bacq, V. Beermann, S. Kuhl, J. Herranz, S. Henning, L. Kuhn, T. Asset, L. Guetaz, G. Renou, J. Drnec, P. Bordet, A. Pasturel, A. Eychmuller, T. J. Schmidt, P. Strasser, L. Dubau and F. Maillard, *Nat. Mater.*, 2018, **17**, 827–833.

167 C. Chen, Y. Kang, Z. Huo, Z. Zhu, W. Huang, H. Xin, J. D. Snyder, D. Li, J. A. Herron, M. Mavrikakis, M. Chi, K. L. More, Y. Li, N. M. Markovic, G. A. Somorjai, P. Yang and V. R. Stamenkovic, *Science*, 2014, **343**, 1339–1343.

168 M. Li, Z. Zhao, T. Cheng, A. Fortunelli, C. Chen, R. Yu, Q. Zhang, L. Gu, B. V. Merinov, Z. Lin, E. Zhu, T. Yu, Q. Jia, J. Guo, L. Zhang, W. A. Goddard Iii, Y. Huang and X. Duan, *Science*, 2016, **354**, 1414–1419.

169 F. Calle-Vallejo, J. Tymoczko, V. Colic, Q. H. Vu, M. D. Pohl, K. Morgenstern, D. Loffreda, P. Sautet, W. Schuhmann and A. S. Bandarenka, *Science*, 2015, **350**, 185–189.

170 L. Dubau, T. Asset, R. Chattot, C. Bonnaud, V. Vanpeene, J. Nelayah and F. Maillard, *ACS Catal.*, 2015, **5**, 5333–5341.

171 M. Lefèvre, E. Proietti, F. Jaouen and J. P. Dodelet, *Science*, 2009, **324**, 71–74.

172 A. Zitolo, V. Goellner, V. Armel, M. T. Sougrati, T. Mineva, L. Stievano, E. Fonda and F. Jaouen, *Nat. Mater.*, 2015, **14**, 937–942.

173 U. Tylus, Q. Jia, K. Strickland, N. Ramaswamy, A. Serov, P. Atanassov and S. Mukerjee, *J. Phys. Chem. C*, 2014, **118**, 8999–9008.

174 G. Wu and P. Zelenay, *Acc. Chem. Res.*, **46**, 1878–1889.

175 C. Duan, J. Tong, M. Shang, S. Nikodemski, M. Sanders, S. Ricote, A. Almansoori and R. O'Hayre, *Science*, 2015, **349**, 1321–1326.

This journal is © The Royal Society of Chemistry 2023

Energy Environ. Sci., 2023, **16**, 4926–4943 | **4943**